RSC Advances

ROYAL SOCIETY OF CHEMISTRY

www.rsc.org/advances

Influence of Ho^{3+} doping in the temperature sensing behavior of Er^{3+}-Yb^{3+} doped La_2CaZnO_5 phosphor

Vijay Kumar[1, 2], S. Som[2, 3], S. Dutta[2], Subrata Das[3*], and H. C. Swart[2*]

[1]Department of Applied Physics, Chandigarh University, Gharuan, Mohali (Punjab)-140413, India

[2]Department of Physics, University of the Free State, Box 339, Bloemfontein 9300, South Africa

[3]Department of Chemical Engineering, National Taiwan University, Taipei, 10617, Taiwan

Tel.: +27-514013852/ +27-58 718 5308; Fax: +27-58 718 444.

E-mail: phy_subrata@yahoo.co.in (S. Das), swarthc@ufs.ac.za (H.C. Swart)

Abstract

In this paper, a series of Er^{3+}/ Yb^{3+} and Er^{3+}/Yb^{3+}/Ho^{3+} codoped La_2CaZnO_5 (LCZ) upconversion (UC) phosphors were synthesized by the combustion route. The UC emission from LCZ phosphors, codoped with fixed Er^{3+}, Ho^{3+}, and various Yb^{3+} concentrations has been investigated. The structural and upconversion properties of the synthesized phosphors were studied in detail. Under 980 nm laser excitation, the codoped samples showed green UC emission that consisted of three well-known emission bands centered at 522, 548 and 672 nm generated by the $^2H_{11/2}\rightarrow{}^4I_{15/2}$, $^4S_{3/2}\rightarrow{}^4I_{15/2}$ and $^4F_{9/2}\rightarrow{}^4I_{15/2}$ transitions of Er^{3+} ions, respectively. The emission intensities of these bands have been enhanced sufficiently on codoping of Yb^{3+} ions in the LCZ: Er^{3+} system. An effort has been presented to explain the enhancement on the basis of a power connection study and an energy level diagram. The luminescence lifetime of the green emission of the LCZ samples with different codoping were also recorded and incorporated to explain the energy transfer

mechanism. The strong temperature dependence of the Fluorescent Intensity Ratio between two green emissions makes the material suitable for temperature sensing purposes and it is also suitable up to high temperatures of 500 K. A relatively high-temperature sensor with good sensitivity 0.00625 K^{-1} was found from the observed results. An increment of 6% for the sensitivity is observed over the existing LCZ phosphor after co-doping with Ho^{3+}. These results indicate that $Er^{3+}/Ho^{3+}/Yb^{3+}$ codoped LCZ material is an effective UC phosphor and may be a potential candidate for high-temperature sensors.

Keywords: Rare earth doped phosphors; upconversion; temperature sensor, optical heater, power dependence; FIR Sensor sensitivity.

Introduction

Rare earth (RE) ions doped upconversion (UC) materials have been the subject of scientific interest due to their significant applications in a variety of fields such as, display devices, temperature sensors, solar cell, bio-imaging, optoelectronics devices, finger print detection, etc.[1-6] Among all these applications, RE-doped UC phosphors based temperature sensors are drawing much attention from the scientific community.[7-8] The traditional temperature sensors are based on a liquid and metal expansion principle; that measure the temperature during the heat flow using an invasive probe.[9] Though, this strategy suffers from some limitations, including spatial resolution, sensitivity and accuracy of detection. This method is also not applicable in many places, such as corrosive environments, coal mines, refineries, etc.[10-12] To overcome these problems, temperature sensing based on a non-contact temperature measurement technique such as infrared (IR) thermometry, Raman spectroscopy, and luminescence can be implemented.[10-11] One practical approach to

measuring the temperature of RE-doped UC materials is the fluorescence intensity ratio (FIR) technique. This method is based on the temperature connection of the FIR between two thermally coupled levels of RE ions as a function of external temperature.[10-12] FIR, in context, is of particular importance for better accuracy, high sensitivity and independence of the measurement conditions.[9-12]

In the last decades, attention has been attracted towards the ternary oxides RE_2MZO_5 (RE = rare earth, M = Ba, Ca, Z = Cu, Zn) based UC and down-conversion materials.[13] RE_2MZO_5 based hosts, in context, are of certain significance due to their excellent structural, physical, chemical, magnetic, optical and superconducting properties. The luminescence properties of La_2BaZnO_5 and Gd_2BaZnO_5 activated with Eu^{3+}, Tb^{3+} and Tm^{3+} were reported for the first time in the year of 1985.[13g] Thereafter, significant research efforts have been directed towards the luminescent properties of RE doped $BaRE_2ZnO_5$ phosphors synthesized by various methods.[13h, 13i] The optical and luminescent properties of La_2CaZnO_5 host doped with different RE ions have been investigated mainly for down-conversion.[14]

The Yb^{3+} ion was demonstrated to be an attractive sensitizer for RE^{3+} ions in various hosts with not only the improved luminescent intensity but also widened excitation spectrum.[2] There are some well-known combinations of the photon energies Er^{3+}–Yb^{3+}, Ho^{3+}–Yb^{3+}, and Tm^{3+}–Yb^{3+}. These combinations were extensively studied by various authors in a significant number of hosts due to their potentiality conversion of the NIR light into visible light. The UC properties of the RE doped systems La_2BaZnO_5 and Gd_2BaZnO_5 have been investigated by Birkel and coworkers.[15] Recent results suggest that the sol-gel derived La_2CaZnO_5: Er^{3+}-Yb^{3+} phosphor is an efficient green UC phosphor.[16] They have also studied optical thermometry in the temperature scale of 298-513 K adopting the FIR technique. But, the internal heating in the material and optical heating generated

by the laser excitation has only been rarely described.[17a] It is worth mentioning that, the interaction between the electron and phonon could be improved by the effect of quantum confinement among phonons, which results in internal heat generation in crystalline phosphors. Therefore, internal heating must be prominent for nanocrystalline solids.[17b] However, the optical heating is related to the interaction between phosphors and the excitation source. When any phosphor material is exposed to the laser irradiation, some portion of the absorbed photons in the phosphor is transformed into heat energy via nonradiative processes owing to which the material gets heated optically.[17c] The nano thermometry behaviour by using the green emissions from Er^{3+} ions in the Er^{3+}-Ho^{3+}-Yb^{3+} triply doped La_2CaZnO_5 (LCZ) phosphors upon NIR excitation have not been investigated at this stage. Moreover, recently, there is a rising interest in the development of temperature sensing technique that is based on the utilization of fluorescent nanomaterials or nanoparticles.[18-19] Vetrone et al.[20] reported that the fluorescent $NaYF_4$: Er^{3+}, Yb^{3+} nanoparticles can be utilized as nanothermometers. They have further stated that the ratio between the green emissions bands of the Er^{3+} ion offers an optical system that in terms regulate temperature distributions in liquids using confocal fluorescence. This opens up the possibility of creating RE^{3+} ions doped UC nanomaterials that can act as thermal probes with interesting applications in biosensors, fluorescent imaging, and therapeutic purposes, etc.[18-20]

In this work, we have focused on the La_2CaZnO_5 host doped with lanthanide ions (Yb^{3+}, Ho^{3+}, Er^{3+}) for strong green and red UC emission properties. An attempt has been made to increase the UC and optical heating performance of the previously reported Yb^{3+}, Er^{3+} codoped material for optical temperature sensing by changing the synthesis condition and the addition of another co-dopant.[16] In this paper, we produced LCZ: Er^{3+}/Ho^{3+}/Yb^{3+} UC phosphors via solution combustion method. Control of crystallization in the phosphors was studied by X-ray diffraction (XRD). The

UC emission characteristics of the synthesized materials have been studied upon 980 nm diode laser excitation at room temperature. The effect of doping and the mechanism involved in the UC process has been studied in detail. The color of the infrared emissions of the codoped sample was also tuned by varying the laser power. Meanwhile, the temperature sensing behavior of the synthesized phosphor has been studied by using FIR of two thermally linked levels of the central UC emission band against 980 nm excitation.

Experimental section

Synthesis of La_2CaZnO_5: Er^{3+}, Ho^{3+}, Yb^{3+} UC phosphors

The La_2CaZnO_5: Er^{3+}, Ho^{3+}, Yb^{3+} UC phosphors (2 mol% Er^{3+}, 2.0-20 mol% Yb^{3+}, 1 mol% Ho^{3+}, respectively) were synthesized via solution combustion route. Analytical reagent (AR) grade lanthanum acetate ($C_6H_9LaO_6$, 99.9%), calcium nitrate ($Ca(NO_3)_2$, >99%), zinc nitrate ($Zn(NO_3)_2$, 97%), erbium nitrate ($Er(NO_3)_3$, 99.9%), holmium nitrate ($Ho(NO_3)_3$, 99.9%), ytterbium nitrate (Yb $(NO_3)_3$, 99.9%) and urea ($CO(NH_2)_2$, >90%) obtained from Sigma-Aldrich were used as the starting raw materials. These materials were taken in the required stoichiometric ratios and mixed properly with deionized water under vigorous stirring condition. When the transparent solution was obtained, the proportionate amount of urea was added to the solution and the solution was stirred for 20 min. Then the solution was transferred in an alumina crucible and kept in a preheated furnace (500 °C) for about 10 min. Within this time, the auto combustion process took place, and a very porous voluminous mass of the powder was formed. The resultant powder was then calcined at 800 °C for 1 h.

Characterizations

X-ray diffraction (XRD) patterns of the as-prepared phosphors were recorded using a Bruker D8 Focus X-ray diffractometer. The scanning electron microscope (SEM) analysis was carried out using a Shimadzu SSX-550. The UC emission and lifetime measurements were performed using the home built setup with a 980 nm laser source. The emitted light was dispersed into a monochromator coupled to a photomultiplier tube through the appropriate lens system. The sample was heated in a home-made furnace and the temperature was controlled by varying the voltage. The temperature was measured with the help of a calibrated thermocouple located in contact with the sample for the temperature sensing investigation. The sample holder along with the sample was kept for 5 min at a constant temperature unless its temperature was stabilized for the upconversion. A common thermometry unit based on phosphors has been illustrated in Scheme 1 schematically. An excitation source (such as LEDs, lasers or flash lamps) is used for the excitation of the phosphor which is attached onto the surface of interest. The resultant emission light passes through an optical filter and is collected in a data acquisition system via an emission detector.

Results and discussion

Structures of the prepared samples

To examine the structure of the LCZ phosphor, the effect of Er^{3+}-doping, Er^{3+}/Yb^{3+} and $Er^{3+}/Yb^{3+}/Ho^{3+}$-codoping in the crystal lattice and to identify the phase, XRD patterns of the UC phosphors were recorded and are shown in Fig. 1. The XRD peak matches well with the LCZ phase as reported elsewhere.[16] The XRD pattern varying dopant and codopant show the same behavior indicating the invariance of the crystal structure after doping and codoping. The crystal system of the prepared samples was identified as a tetragonal structure with space group P 4/mmm (no. 123) having lattice parameters a=b= 7.0837 Å, c= 11.884 Å and α=β= γ= 90°. It is evident

from the existing literature that the iso-structures such as $BaLa_2ZnO_5$ and $BaNd_2ZnO_5$ derived via the sol-gel method follow the same tetragonal behavior. [13a, 14a, 16]

Structure formation and unit cell

Rietveld refinement of long scan XRD patterns of undoped La_2CaZnO_5 was carried out and a part is shown here in Fig. 2(a) in the range~ 20°- 80°. The refinement was carried out by FullProf software using the XRD data. The experimental diffraction data is shown by black line. The "×" marks represent the simulated diffraction data. The blue line indicates how much the calculated data deviates from the original values. If this line will be straight it will be perfect matching. In the present case small noise in the blue line indicates good matching for this refinement. The eminence of refinement can be quantified by some factors obtained during refinement known as reliability factors. Reliability factor includes factor for the weighted pattern (R_{wp}), factor for the pattern (R_p), and the goodness-of-fit indicator (s). For good refinement, R_p and R_{wp} must be less than 10% and s must approach to unity. In the present case, the parameters were found to be well within the range of a good fitting as summarized in Table 1. The estimated reliability factors verified that the pure phases were obtained without impurities. The crystal system of the prepared samples was identified as a tetragonal structure with space group P 4/mmm (no. 123) having lattice parameters a=b= 7.0837 Å, c= 11.884 Å and α=β= γ= 90°. The structural parameters obtained from the Rietveld analysis of the La_2CaZnO_5 phases are listed in Tables 1. The refined structural parameters show good agreement with the previous work. [13a, 13h, 14a, 16] The structure of the undoped LCZ was estimated via the VESTA software using the data obtained from the Rietveld refinement as shown in Fig. 2(b). The crystal structure of La_2CaZnO_5 is composed of three polyhedral LaO_8, CaO_{10} and ZnO_4 and the composition of three different polyhedra is schematically shown in Fig. 2(b).

UC emission study

The UC of the as-synthesized LCZ: Er^{3+}/Yb^{3+} phosphors were recorded as a function of different Yb^{3+}-codoping concentrations and the corresponding results are shown in Fig. 3.

As shown in Fig. 3, three sensitized UC emission bands centered at 523, 548 and 672 nm were observed in the case of 2 mol% Er^{3+} doped LCZ phosphor. These bands corresponded to the transitions of Er^{3+} ions: $^2H_{11/2} \rightarrow {}^4I_{15/2}$, $^4S_{3/2} \rightarrow {}^4I_{15/2}$ and $^4F_{9/2} \rightarrow {}^4I_{15/2}$, respectively. [16, 21-22] With the increase in Yb^{3+} concentration the UC intensity was seen to increase and at the concentration of 2 mol% Er^{3+} and 5 mol% of Yb^{3+} the UC intensity reached a maximum. When the Yb^{3+} concentration was incorporated and increased, the green and red emission of Er^{3+} increased significantly, suggesting the appreciable energy transfer process between sensitizers (Yb^{3+}) to the activators (Er^{3+}). The Yb^{3+} ion has a pretty long absorption energy level ($^2F_{5/2} \rightarrow {}^2F_{7/2}$) at 980 nm excitation wavelength. Therefore, upon excitation with 980 nm, apart from excited state absorption (ESA), an adequate energy transfer (ET) from Yb^{3+} to Er^{3+} could be conceivable due to spectral overlap between the Yb^{3+} transition of $^2F_{5/2} \rightarrow {}^2F_{7/2}$ and that of Er^{3+} absorption energy $^4I_{11/2} \rightarrow {}^4I_{15/2}$, which significantly increased the UC intensity. This is clearly shown in the energy-level diagram explained later. The digital image of the green colour emission is shown in the inset of Fig. 3.

Figure 4 shows the UC spectra of LCZ: 2 mol% Er^{3+}/ 5 mol% Yb^{3+}, LCZ: 1 mol% Ho^{3+}/ 5 mol% Yb^{3+} and LCZ: 2 mol% Er^{3+}/ 1mol% Ho^{3+}/ 5 mol% Yb^{3+} phosphors. It is obvious that the green emission was more intense in the triply doped sample than that of other samples, which indicates efficient energy transfer between Yb^{3+}, Er^{3+} and Ho^{3+} and the energy transfer mechanisms will be discussed later. The enhancement of UC emission after codoping with Ho^{3+} has been reported in other papers.[23-24] To confirm the energy transfer phenomena the lifetime of the green emission of the LCZ samples with codoping ratio Er: Ho: Yb as 0:1:0, 0:1:5, 2:0:0, 2:0:5 and 2:1:5 were

recorded and are shown in Fig. 5. The resulting decay curves were found to follow the double exponential nature as per the following equation: [25a]

$$I(t) = I_1 e^{-t/\tau_1} + I_2 e^{-t/\tau_2} \quad (1)$$

where *I(t)* represents the intensity of luminescence at a particular time, and τ_1 and τ_2 are the short and long lifetimes that correspond to the intensity coefficients I_1 and I_2, respectively. The average lifetime was then estimated using the formula [25a] $\tau_{av} = (I_1\tau_1^2 + I_2\tau_2^2) / (I_1\tau_1 + I_2\tau_2)$. The multiexponential decay response designates the inhomogeneous dispersion of the doping ions in the host material pointing to the change in the local concentration or the shift of excitation energy from a contributor to lanthanide activators.[25a] However, the green emission lifetime increased after the codoping of Yb^{3+} in both the doping separately. In case of triply doping phosphor, the lifetime was obtained to be a maximum of 137 μs. This phenomenon confirmed the presence of ET from Yb^{3+} to Er^{3+}/ Ho^{3+} in the present host matrix.

In this research, it is proven that $Ho^{3+}/Yb^{3+}/Er^{3+}$ and Er^{3+}/Yb^{3+} codoping samples are both suitable for UC emission by pumping at 980 nm, but the triply doped sample was even better. The close vicinity of the individual energy levels of these three ions make the energy transfer processes possible. To understand the mechanism precisely the UC intensity was recorded of LCZ: 2mol%Er^{3+}/ 5mol% Yb^{3+} phosphor by varying the laser power (P). The intensity was seen to increase with the increase in P as shown in Fig. 6(a). Fig. 6(b) displays the similar increment behavior of the UC intensity of the LCZ: 2mol%Er^{3+}/ 1mol% Ho^{3+}/ 5mol% Yb^{3+} phosphor while varying the laser power (P).

The variation colour coordinate of LCZ: 2 mol%Er^{3+}/ 5 mol% Yb^{3+} phosphor with P is shown in the Commission Internationale de L'Eclairage (CIE) chromaticity diagram of Fig. 7 (a). The

similar variation of colour coordinate from the yellowish green region towards the deep green region with the increase in pump power was also observed in the case of the LCZ: 2mol%Er^{3+}/ 1mol% Ho^{3+}/ 5mol% Yb^{3+} phosphor as is shown in Fig. 7 (b). It is well accepted that the temperature has been changed by varying the excitation power density, which in turn affect the emission intensities and colors. In this present research, the above possibility has been examined for LCZ: Er/ Yb and LCZ: Er/ Ho/ Yb phosphors by measuring their emission colour and corresponding CIE coordinates as a function of different pump-power densities, as shown in Fig. 7. It shows that pump-power/temperature has a significant effect on the chromaticity coordinates, as a variation of colour coordinate from the yellowish green region towards the deep green region with the increase in pump power was observed in the case of the LCZ: 2 mol%Er^{3+}/ 5 mol% Yb^{3+} and LCZ: 2 mol%Er^{3+}/ 1 mol% Ho^{3+}/ 5 mol% Yb^{3+} phosphors as shown in Fig. 7 (a) and (b), respectively. Such variation in the CIE or emission colour may be accounted for due to the different saturation behavior of the green and red emissions of Er^{3+} and Ho^{3+} ions.[25b] The colour changing property of the present UC phosphors with the variation of power/temperature directly indicated their suitability for thermometry applications in which the emission of a phosphor need to be modulated very precisely under temperature variations.

The intensity of the UC bands $(I_{emission})$ follows the relation: $I_{emission} \propto P^n$, where n denotes the number of incident photons involved in the UC emission. [16, 21-22] The n value can be determined from the slope of the linear fitting between *logI vs. logP* as shown in Fig. 8. The straight line plot for three different bands and the slope (n) for LCZ: 2mol%Er^{3+}/ 5mol% Yb^{3+} phosphors are found as 1.79 and 2.02 for the green transitions at 522, and 548 nm, and 2.48 for the red transition at 672 nm as shown in Fig. 8 (a). In the case of LCZ: 2mol%Er^{3+}/ 1mol% Ho^{3+}/ 5mol% Yb^{3+} phosphor the n value was obtained as 1.51 and 2.05 for the green transitions at 522, and 548 nm, and 1.99

for the red transition at 672 nm as shown in Fig. 8 (b). The n values are much larger than 2 and revealed that two and three IR photons are involved in producing one green (548 nm) or red (672 nm) photon in this UC process, and the n values are close to 2 in the case of the 522 nm band, which indicates the involvement of two-photons as clearly explained in the literature.[16]

The energy level diagram showing the probable mechanism and population processes in LCZ: Er^{3+}/ Ho^{3+}/ Yb^{3+} UC phosphor is schematically shown in Fig. 9. [16, 21-22] The details of the different energy transfer processes in the present system were reported recently.[16] The involved possible energy transfer mechanisms from Yb^{3+} and Er^{3+} to Ho^{3}+ for the UC emission are discussed below based on the energy level diagram showed in Fig. 9. First, the $^2F_{7/2}$ level of Yb^{3+} is excited to the $^2F_{5/2}$ level by ground state absorption (GSA) when the sample is pumped by 980 nm laser and then can transfer their energy to the Ho^{3+}: $^5I_6$ and Er^{3+}: $^4I_{11/2}$ levels. GSA can also occur for Er^{3+}: $^4I_{15/2}$ → $^4I_{11/2}$ when pumped by 980 nm laser. However, compared with the ground state absorption of Ho^{3+}/ Er^{3+}, Yb^{3+} ions possess a larger absorption cross-section at 980 nm and ion concentration, and energy transfer occurs efficiently as a result of the large spectral overlap between the Yb^{3+} emission $^2F_{5/2}$–$^2F_{7/2}$ and the Er^{3+} absorption $^4I_{15/2}$–$^4I_{11/2}$ (ET1) or Ho^{3+} absorption $^5I_8$–$^5I_6$ (ET2) bands. Because the energy gap (1040 cm^{-1}) of the ET2 process is larger than that (432 cm^{-1}) of the ET1 process, the energy transfer efficiency of ET1 is expected to be higher than that of ET2. Thus, ET1 can promote the Er^{3+} ion from the $^4I_{15/2}$–$^4I_{11/2}$ state, and if the latter is previously populated, the Er^{3+} ion may transit from the $^4I_{11/2}$ to the $^4F_{7/2}$ and from $^4F_{7/2}$ to $^4G_{11/2}$ states. Succeeding nonradiative relaxations could fill the $^2H_{11/2}$ and $^4S_{3/2}$ states that are the emitting levels for the green luminescence.

The $^4I_{11/2}$ states of Er^{3+} ions could be eliminated by an alternative relaxation process to $^4I_{13/2}$ states, which may be further stimulated to the red emitting levels $^4F_{9/2}$, and the identical transition to the

ground state $^4I_{15/2}$ gives red emission. In case of the Ho^{3+} ion, ET2 populated the $^5I_6$ state of the Ho^{3+} ion which further promote the Ho^{3+} ion from the $^5I_6$ –$^5F_4$ state and the $^5F_4$ state is the emitting levels for the green luminescence. If the $^5I_6$ state of the Ho^{3+} ion depopulated by a nonradiative relaxation route to the $^5I_7$ state, it can be excited to the $^5F_5$ state of the Ho^{3+} ion which is the red emitting level.

But due to the stronger UC emission of $Ho^{3+}/Er^{3+}/Yb^{3+}$ triply doped sample compared to other codoped samples, it can be inferred that there may exist some energy transfer process between the Er^{3+} and Ho^{3+} ions. The spectral overlap between the Er^{3+} emission $^4S_{3/2}$–$^4I_{15/2}$ and the Ho^{3+} absorption $^5F_4$–$^5I_8$ supports this conclusion. When Ho^{3+} ion is codoped in the LCZ: Er/ Yb phosphor, the density of the Er^{3+} ions increases in the $^4S_{3/2}$ level and hence the green (~548 nm) emission increases. [16, 23-24] The possible energy migrations between Ho^{3+} and Er^{3+} can be verified via a comparative UC emission spectra of LCZ: Er/ Yb, LCZ: Ho/ Yb and LCZ: Er/ Ho/ Yb, as shown in Fig. 4. Substantial increase in the green–red intensity (I_{548nm}/I_{672nm}) ratio from 1.78 to 2.36 with the incorporation of Ho^{3+} in LCZ: Er/ Yb directly indicates the possible energy transfer between Er^{3+} and Ho^{3+}. Now, the energy transfer process from Ho^{3+} to Er^{3+} in LCZ: Er/ Ho/ Yb phosphor can be clearly confirmed from the lifetime analysis. The decay time for the 548 nm green emission were estimated to be 109, 113 and 137 μs for LCZ: Er/ Yb, LCZ: Ho/ Yb and LCZ: Er/ Ho/ Yb, respectively. As illustrated Fig. 5, an increment in the decay time for LCZ: Er/ Ho/ Yb could be due to the energy transfer process from Ho^{3+} to Er^{3+}. Nevertheless, $^4S_{3/2}\rightarrow{}^4I_{15/2}$ and $^4F_{9/2}\rightarrow{}^4I_{15/2}$ transitions (548 and 672 nm, respectively) of Er^{3+} ions are significantly overlapped with that of $^5S_2$, $^5F_4\rightarrow{}^5I_8$ and $^5F_5\rightarrow{}^5I_8$ transitions (546 and 661 nm, respectively) of Ho^{3+} ions, as illustrated in Fig. 9. Owing to such overlapping, probabilities of energy transfer from Ho^{3+} and

Er^{3+} enhanced. Therefore, it is predicted that such energy transfer phenomena may enhanced the green emission intensity and its life time in LCZ: Er/ Ho/ Yb.

Temperature sensing ability

The temperature sensing study of UC emission spectra of the green bands from 300 K to 573 K of Er^{3+}/ Yb^{3+} codoped) and Er^{3+}/ Ho^{3+}/ Yb^{3+} codoped (triply doped) LCZ phosphor have been performed with 980 nm excitation and are shown in Figs. 10 and 11, respectively. From both the figures, it is observed that on increasing the sample temperature, the band positions remain unchanged, but the integrated intensity of two green bands changed in a reverse way. At room temperature (300 K), the intensity corresponding to the $^2H_{11/2} \rightarrow {}^4I_{15/2}$ transition was lower than that of the $^4S_{3/2} \rightarrow {}^4I_{15/2}$ transition. While at a higher temperature (573 K), the reverse effect was observed.

This variation in the intensity of the two bands that increased their intensity ratio (I_{522nm}/I_{548nm}) as a function of temperature was caused due to the change in their relative population.[16] The ratio is called the Fluorescent Intensity ratio (FIR) and the variation of FIR with temperature for both the sample is shown in Fig. 12.

As, the population of these two thermally coupled levels follows the Boltzmann's distribution, the FIR of these transitions can be used for optical thermometry via the relation:

$$FIR = I_{522}/I_{548} = C \exp(-\Delta E/kT) \quad (2)$$

where I_{522} and I_{548} are the integrated intensities corresponding to the $^2H_{11/2} \rightarrow {}^4I_{15/2}$ and $^4S_{3/2} \rightarrow {}^4I_{15/2}$ transitions, respectively; C is a pre-exponential constant; ΔE is the energy difference between the $^2H_{11/2}$ and $^4S_{3/2}$ levels; k is Boltzmann's constant and T is the absolute temperature.[16]

The linear conversion of equation (2) can be written as

$$\ln(I_{522}/I_{548}) = -(\Delta E/k)(1/T) + \ln(C) \quad (3)$$

The corresponding energy difference ΔE can be calculated from the slope (ΔE/k) of the linear fitting of $\ln(I_{525nm}/I_{548nm})$ versus 1/T plot as shown in Fig. 13. The fitting of the experimental data gives a slope of about 640.53 and 1168.85 for codoped and triply doped phosphors respectively and resulting in an energy difference ΔE of about 444 and 810 cm^{-1}.[16] The performance of the temperature sensor generally depends on the figure of merit of the sensing behavior. The figure of merit includes different parameters such as absolute sensitivity (S_a), relative sensitivity (S_r) and the resolution. The absolute sensitivity is defined as the variation of the FIR or lifetime (for two approaches) with respect to temperature and is expressed as[26]:

$$S = dR/dT = FIR(-\Delta E/kT^2) \quad (4)$$

where *S* is the sensor sensitivity and the other terms have their usual meanings.[9]

The absolute sensor sensitivity in the present case was calculated for the FIR measurements and was obtained as 0.0029 and 0.0047 K^{-1} at 300 K for the codoped and the triply doped phosphors, respectively and then increased with the rise in temperature. The maximum sensitivity was observed as 0.0036 at 348 K for the codoped phosphor whereas 0.0067 at 398 K for the triply doped phosphor. The sensitivity value was higher in the case of the triply doped sample. This is because after codoping of Ho^{3+}, the Boltzmann population of the Er^{3+} ion increased in the $^4S_{3/2}$ state. Therefore, the intensity ratio between the transition from $^2H_{11/2}$ and $^4S_{3/2}$ state to ground state as well as the FIR were modified, which affected the sensitivity.[27] As illustrated in the energy diagram (Fig. 9), UC initiates through Yb^{3+} sensitizer excitation and ET to Er^{3+} and Ho^{3+} ions and consequently favors the simultaneous inter-ion ET between Er^{3+} and Ho^{3+} ions. Moreover, excited

state absorption (ESA) and cross-relaxation (CR) processes in both Er^{3+} and Ho^{3+} ions significantly improve the UC efficiency. Now, as we know that the temperature sensitivity is depended on the FIR which is defined as the intensity ratio of the emission intensities centered at 525 nm and 548 nm. Due to the incorporation of Ho in the Er/Yb codoped system, this ratio has been changed and it is found that the FIR values of Er/Yb/Ho codoped system changed more systematically owing to which the sensitivity was increased.

With the further increase in temperature the sensitivity decreased for both the cases. The variation of absolute sensitivity with temperature for FIR measurement is shown in Fig. 14. This figure shows that the sensitivity increased after codoping of Ho^{3+} in the LCZ: Er^{3+}/ Yb^{3+} phosphor. The relative sensor sensitivity is the normalized absolute sensor sensitivity with respect to the measured value. The equation 5 is used to calculate the relative sensitivity as per the following equation:[28-29]

$$S_r = \left| \frac{1}{FIR} \frac{\partial(FIR)}{\partial T} \right| \times 100\% \quad (5)$$

Fig. 15 indicates that the relative sensor sensitivity values decreased with temperature in the measured range. However, the values are sensibly higher than the reported over the examined large temperature range from room temperature to the higher temperatures. This behavior indicates the suitability of this material as an attractive host in the operation of electronic devices for temperature sensing purposes. The maximum relative sensor sensitivity value is 0.71 $\%K^{-1}$ and 1.52 % K^{-1} at 300 K for the codoped and the triply doped phosphors respectively.

The effect of Ho^{3+} concentration on the experimentally estimated sensitivity was determined for the 300- 573 K temperature range and the variation of the maximum relative sensitivity at 300 K with Ho^{3+} concentration is presented in Fig. 16. The figure shows that with an increase of the Ho^{3+}

ions amount from 1 to 9 mol% the relative sensitivity decreased exponentially from 1.52% K^{-1} to 0.28% K^{-1}. This effect can be explained via the energy transfer phenomena between Ho^{3+} ions. With the increment of Ho^{3+} concentration, the cross relaxation $[^5F_4,^5I_8] \rightarrow [^5I_5,^5I_7]$ between Ho^{3+} ions starts which leads to lowering of the $^2H_{11/2}$ state population of Er^{3+} and hence $^2H_{11/2} \rightarrow {}^4I_{15/2}$ emission intensity. The probability of this energy transfer increases with the reduction of the average distance between these ions connected. Therefore, the cross relaxation process will affect the changes of FIR and hence the relative sensitivity. Marciniak et al.[30] has observed the similar behaviour in the case of Er: $LiYbP_4O_{12}$ luminescent thermometer.

A comparison of relative sensor sensitivity value and the temperature range between the recently developed Ln^{3+} phosphor based inorganic nano-thermometers is summarized in Table 2 and it indicates that the relative sensor sensitivity value in case of the present phosphor is among the highest.

Temperature resolution is also an important factor to characterize any temperature sensor devices and can be defined to the minimal detectable signal change. The standard deviation data of residuals in the fit of the experimental FIR data points with temperature and the absolute sensitivity were used to estimate resolution as the method described by Brites et al.[18] and the estimated resolutions of FIR temperature sensing is shown in Fig. 17.

Both the curve follows similar behavior and it is observed that the FIR measurements for the codoped phosphors provided better resolution compared to the triply doped sample. The resolution values in both the cases are very much lower than 1K over a large temperature range from 300 K to 573K. The maximal resolutions were obtained at 325 K for the codoped phosphor as 0.105 K and at 425 K for the triply doped sample 0.115 K. The comparative sensitivity data and resolution behavior of the LCZ: Er/ Ho/ Yb phosphor with the other phosphor indicates the suitability of this

material for temperature sensing application. Similar studies have been reported by Li and co-workers for sol-gel derived Yb^{3+}-Er^{3+} co-doped La_2CaZnO_5 phosphors, with a sensitivity of 0.0059 K^{-1} at 483K.[16] But the FIR at 483K is about 1.15. This indicates the Sr value is about 0.51 $\%K^{-1}$. Similar studies were also carried out by various authors for different materials.[9, 17] In the present case for the sample LCZ: Er/ Yb the sensitivity was observed as 0.0036 K^{-1} at 348 K. This value has increased by above 69% after codoping of Ho^{3+}, which is about 7% greater than the reported one. The obtained relative sensitivity is higher than the reported. And also, the resolution is very much lower than 1 K over a large temperature range from 300 K to 573K. The results imply that the studied UC phosphor is superb for temperature sensing applications.

Conclusions

In summary, a series of Er^{3+}/Yb^{3+} and $Er^{3+}/Ho^{3+}/Yb^{3+}$ codoped $La_2Ca_2ZnO_5$ phosphors were prepared by the combustion synthesis method. The crystal system of the prepared samples was identified as a tetragonal structure and the doping of RE ions did not affect the crystal structure. Under the laser excitation of 980 nm, the Er^{3+}/Yb^{3+}-codoped sample exhibited strong green and red UC emissions from $^2H_{11/2}$, $^4S_{3/2}\rightarrow{}^4I_{15/2}$ and $^4F_{9/2}\rightarrow{}^4I_{15/2}$ transitions of Er^{3+} ions, respectively. The enhanced UC emission after codoping of Ho^{3+} was explained on the basis of energy exchange mechanisms between Er^{3+}/ Ho^{3+} and Yb^{3+} ions. Power dependence studies infer that the UC bands arose through a two/ three-photon absorption process. The high corresponding sensor responsiveness over a broad temperature range with large temperature resolution make the phosphors suitable for future applications in thermometry. The FIR technique was used to measure the sensitivity of the synthesized temperature sensors, and it can be concluded that at 400 K the obtained phosphors shows a relatively higher sensitivity and resolution over the existing one.

These data indicate the suitability of LCZ: Er^{3+}/ Ho^{3+}/ Yb^{3+} phosphors for temperature sensor applications.

Acknowledgments

Dr. Vijay Kumar is greatly acknowledged the Science and Engineering Research Board (SERB), New Delhi for financial assistance in the form of Young Scientist Scheme (Fast Track; File No. DST No: SB/FTP/ETA-215/2014). The financial assistance from the University of the Free State is also highly recognized.

References

1 H.-Q. Wang, M. Batentschuk, A. Osvet, L. Pinna and C. J. Brabec, *Adv. Mater.*, 2011, **23**, 2675-2680.

2 J. C. Ruiz-Morales, J. Mendez-Ramos, P. Acosta-Mora, M. E. Borgesc and P. Esparza, *J. Mater. Chem. C*, 2014, **2**, 2944-2948.

3 R. Martin-Rodríguez, R. Valiente, S. Polizzi, M. Bettinelli, A. Speghini and F. Piccinelli, *J. Phys. Chem. C*, 2009, **113** (28), 12195–12200.

4 Y. Tian, B. Tian, C. Cui, P. Huang, L. Wang and B. Chen, *RSC Adv.*, 2015, **5**, 14123-14128.

5 (a) W. Xu, Z. G. Zhang and W. W. Cao, *Opt. Lett.*, 2012, **37**, 4865-4867. (b) R. Dey, A. Kumari, A. K. Soni, V. K. Rai, *Sens. Actuator. B*, 2015, **210**, 581. (c) A. K. Soni, V. K. Rai, S. Kumar, *Sens. Actuator. B*, 2016, **229**, 476. (d) A. K. Soni, V. K. Rai, *Dalton Trans.*, 2014, 43, 13563.

6 (a) G. Ajithkumar, B. Yoo, D. E. Goral, P. J. Hornsby, A.-L. Lin, U. Ladiwala, V. P. Dravide and D. K. Sardar, *J. Mater. Chem. B*, 2013, **1**, 1561-1572. (b) S. P. Tiwari, K. Kumar, V. K. Rai, *J. Appl. Phys.*, 2015, **118**, 183109.

7 J. Chen and J. X. Zhao, *Sens.*, 2012, **12**, 2414-2435.

8 B. Dong, B. Cao, Y. He, Z. Liu, Z. Li and Z. Feng, *Adv. Mater.*, 2012, **24**, 1987-1993.

9 B. P. Singh, A. K. Parchur, R. S. Ningthoujam, P. V. Ramakrishna, S. Singh, P. Singh, S. B. Rai and R. Maalej, *Phys. Chem. Chem. Phys.*, 2014, **16**, 22665-22676.

10 S. Zhou, K. Deng, X. Wei, G. Jiang, C. Duan, Y. Chen and Min Yin, *Opt. Commun.*, 2013, **91**, 138-142.

11 H. Zheng, B. Chen, H. Yu, J. Zhang, J. Sun, X. Li, M. Sun, B. Tian, H. Zhong, S. Fu, R. Hua and H. Xia, *RSC Adv.*, 2014, **4**, 47556.

12 (a) X. Yang, Z. Fu, Y. Yang, C. Zhang, Z. Wu and T. Sheng, *J. Amer. Cer. Soc.*, 2015, **98**, 2595. (b) V. K. Rai, Appl. Phys. B, 2007, **88**, 297. A. K. Soni, R. Dey, V. K. Rai, RSC Adv., 2015, 5, 34999. (c) A. Kumar, S. P. Tiwari, K. Kumar, V. K. Rai, Spectroch. Acta Part A: Molecul. Biomol. Spectr., 2016, **167**, 134.

13 (a) I. Etchart, M. Berard, M. Laroche, A. Huignard, I. Hernandez, W. P. Gillin, R. J. Curry and A. K. Cheetham, *Chem. Commun.*, 2011, **47**, 6263–6265. (b) B. N. Tian, B. J. Chen, Y. Tian, J. S. Sun, X. P. Li, J. S. Zhang, H. Y. Zhong, L. H. Cheng, Z. L. Wu and R. N. Hua, *Ceram. Int.*, 2012, **38**, 3537–3540. (c) A. Jaffres, B. Viana and E. van der Kolk, *Chem. Phys. Lett.*, 2012, **527**, 42–46. (d) I. Etchart, I. Hernandez, A. Huignard, M. Berard, M. Laroche, W. P. Gillin, R. J. Curry and A. K. Cheetham, *J. Appl. Phys.*, 2011, **109**, 063104. (e) C.-H. Liang, Y.-C. Chang and Y.-S. Chang, *J. Electrochem. Soc.*, 2009, **156**, J303. (f) L. Shi and H. J. Seo, *J. Lumin.*, 2011, **131**, 523–525. (g) M. J. J. Lammers, H. Donker and G. Blasse, *Mat. Chem. Phys.*, 1985, **13**, 527-529. (h) J. Xie,L. Mei, L. Liao, M. Guan, H. Liu, *J. Phys. Chem. Solids*, 2015, **83**, 152-156. (i) A. Yoshida, H. Ogawa, A. Kan and T. Kondo, *J. Eur. Cer. Soc.*, 2005, **25**, 2897–2900.

14 (a) V. R. Bandi, B. K. Grandhe, K. Jang, H.-S. Lee, D.-S. Shin, S.-S. Yi and J.-H. Jeong, *J. Alloys Comp.*, 2012, **512**, 264– 269. (b) H. J. Woo, V. R. Bandi, B. K. Grandhe, K. Jang, J. Park, J. Yoon, H. S. Lee, D. H. Bae, S. S. Yi and J. H. Jeong, *J. Nanosci. Nanotechnol.*, 2013, **13**(2), 848-852.

15 A. Birkel, A. A. Mikhailovsky and A. K. Cheetham, *Chem. Phys. Lett.*, 2009, **477**, 325–329.

16 L. Li, C. Guo, S. Jiang, D. K. Agrawal and T. Li, *RSC Adv.*, 2014, **4**, 6391.

17 (a) A. Pandey, S. Som, V. Kumar, V. Kumar, K. Kumar, V.K. Rai, and H.C. Swart, *Sens. Actuator. B*, 2014, **202**, 1305. (b) H. Suo, C. Guo, Z. Yang, S. Zhou, C. Duan, M. Yin, *J. Mater. Chem. C*, 2015, **3**, 7379. (c) S. K. Singh, K. Kumar, S. B. Rai, *Appl. Phys. B*, 2010, **100**, 443.

18 C. D. S. Brites, Patricia P. Lima, Nuno J. O. Silva, Angel Millan, Vitor S. Amaral, Fernando Palacio, Luıs D. Carlos, *Nanoscale*, 2012, **4**, 4799.

19 D. Jaque and F. Vetrone, *Nanoscale*, 2012, **4**, 4301.

20 F. Vetrone, R. Naccache, A. Zamarron, A. J. de la Fuente, F. Sanz-Rodrıguez, L. M. Maestro, E. M. Rodriguez, D. Jaque, J. G. Sole, J. A. Capobianco, *ACS Nano* 2014, **4**, 3254-3258.

21 W. Xu, Z. G. Zhang and W. W. Cao, *Opt. Lett.*, 2012, **37**, 4865-4867.

22 J. S. Wang, D. P. Machewirch, F. Wu, E. M. Vogel and E. Snitzer, *Opt. Lett.*, 1994, **19**, 1448-1149.

23 R. Xu, J. Pan, L. Hu and J. Jhang, *J. Appl. Phys.* 2010, **108**, 043522-043527.

24 Y. Tian, I. hang, S. Feng, R. Xu, L. Hu and J. Jhang, *Opt. Mater*. 2010, **32**, 1508- 1513.

25 (a) S. Dutta, S. Som and S. K. Sharma, *RSC Adv.*, 2015, **5**, 7380. (b) Subrata Das, A. Amarnath Reddy, S. Surendra Babu, G. Vijaya Prakash, *Mater. Lett.*, 2014, **120**, 232.

26 S. A. Wade, S. F. Collins and G. W. Baxter, *J. Appl. Phys.*, 2003, 94, 4743.

27 H. Zheng, B. Chen, H. Yu, J. Zhang, J. Sun, X. Li, M. Sun, B. Tian, H. Zhong, S. Fu, R. Hua and H. Xia, *RSC Adv.*, 2014, **4**, 47556- 47563.

28 C. H. Hsia, A. Wuttig and H. Yang, ACS Nano, 2011, 5, 9511–9522.

29 E. J. McLaurin, V. A. Vlaskin and D. R. Gamelin, *J. Am. Chem. Soc.*, 2011, 133, 14978–14980

30 L. Marciniak, K. Waszniewska, A. Bednarkiewicz, D. Hreniak and W. Strek, *J. Phys. Chem. C., (Accepted)* ***DOI:*** *10.1021/acs.jpcc.6b01636*

31 N. N. Dong, M. Pedroni, F. Piccinelli, G. Conti, A. Sbarbati, J. E. Ramirez-Hernandez, L. M. Maestro, M. C. Iglesias-de la Cruz, F. Sanz-Rodriguez, A. Juarranz, F. Chen, F. Vetrone, J. A. Capobianco, J. G. Sole, M. Bettinelli, D. Jaque and A. Speghini, *ACS Nano*, 2011, **5**, 8665–8671.

32 S. K. Singh, K. Kumar and S. B. Rai, *Sens. Actuators, A*, 2009, **149**, 16–20.

33 E. Saidi, B. Samson, L. Aigouy, S. Volz, P. Low, C. Bergaud and M. Mortier, *Nanotechnology*, 2009, **20**, 115703.

34 X. Wang, X. G. Kong, Y. Yu, Y. J. Sun and H. Zhang, *J. Phys. Chem. C*, 2007, **111**, 15119-15124.

Figure captions:

Scheme 1: Schematic diagram for temperature sensing.

Fig. 1 XRD pattern of LCZ phosphor with varying RE concentration.

Fig. 2 (a) Fitted (×) and original (black line) powder XRD pattern of La_2CaZnO_5 phosphors and residuals (blue line in the bottom) for the structure refinement by the Rietveld method using the

EXPO Program. (b) Schematic diagram of the La_2CaZnO_5 complex structure drawn by VESTA software.

Fig. 3 UC spectra of LCZ phosphor with varying Er/ Yb concentration.

Fig. 4 Comparative UC spectra of LCZ phosphor with varying Er/ Ho/ Yb concentration.

Fig. 5 Decay intensity as function of time of the green emission of the LCZ samples with different codoping ratios.

Fig. 6 Variation of UC intensity with the increment of the Laser Power for (a) LCZ: Er/ Yb and (b) LCZ: Er/ Ho/ Yb phosphors.

Fig. 7 Variation of colour coordinates with the increment of Laser Power for (a) LCZ: Er/ Yb and (b) LCZ: Er/ Ho/ Yb phosphors.

Fig. 8 Dependence of UC intensity with pumping Power for (a) LCZ: Er/ Yb and (b) LCZ: Er/ Ho/ Yb phosphors.

Fig. 9 Energy level diagram of Er^{3+}, Ho^{3+} and Yb^{3+} ions for various emissions of the La_2CaZnO_5 phosphor.

Fig. 10 Variation of UC spectra with temperature for La_2CaZnO_5: Er^{3+}/Yb^{3+} phosphor.

Fig. 11 Variation of UC spectra with temperature for La_2CaZnO_5: Er^{3+}/ Ho^{3+}/ Yb^{3+} phosphor.

Fig. 12 Variation of FIR value of the green emission in LCZ host with different doping as a function with temperature.

Fig. 13 Variation of FIR value of the green emission in the LCZ host with temperature.

Fig. 14 Variation of absolute sensor sensitivity of the LCZ phosphors with temperature.

Fig. 15 Variation of relative sensor sensitivity of the LCZ phosphors with temperature.

Fig. 16 Variation of relative sensor sensitivity of the LCZ phosphors with Ho^{3+} concentration.

Fig. 17 Variation of resolution of the LCZ temperature sensor with temperature.

Table captions:

Table 1: Refinement parameter obtained from FullProf Software.

Table 2 Comparative analysis of relative sensitivity and temperature range of the inorganic sensor materials.

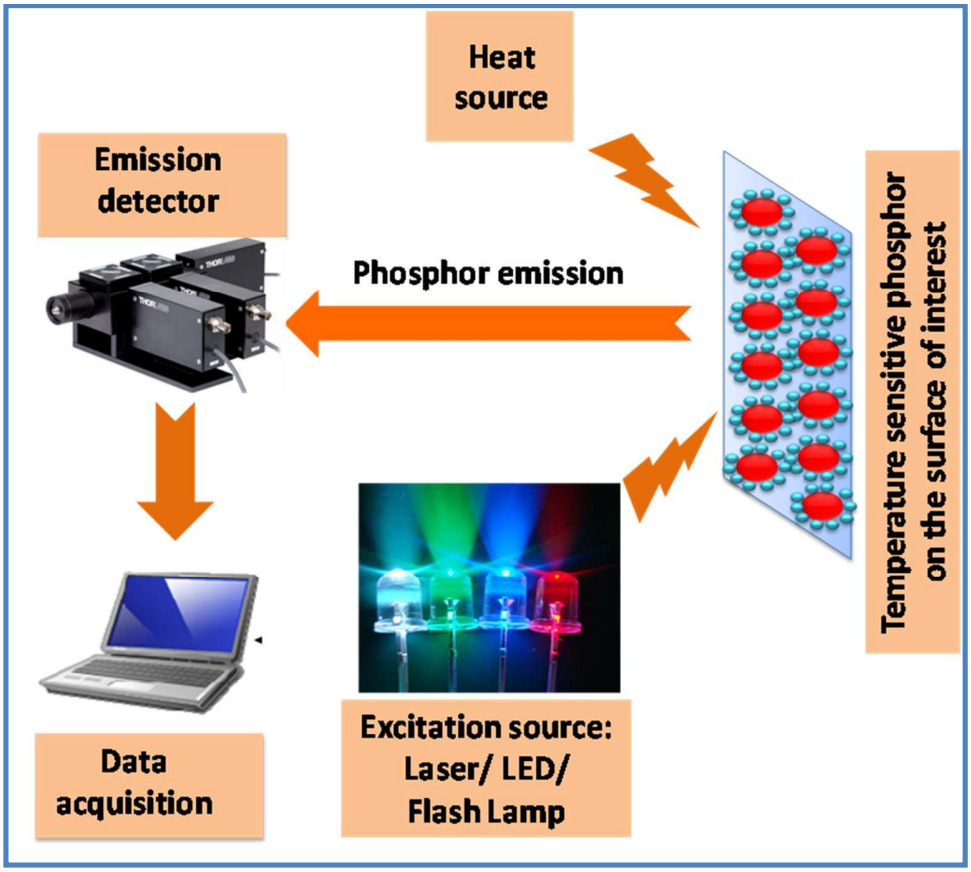

Scheme 1: Schematic diagram for temperature sensing.

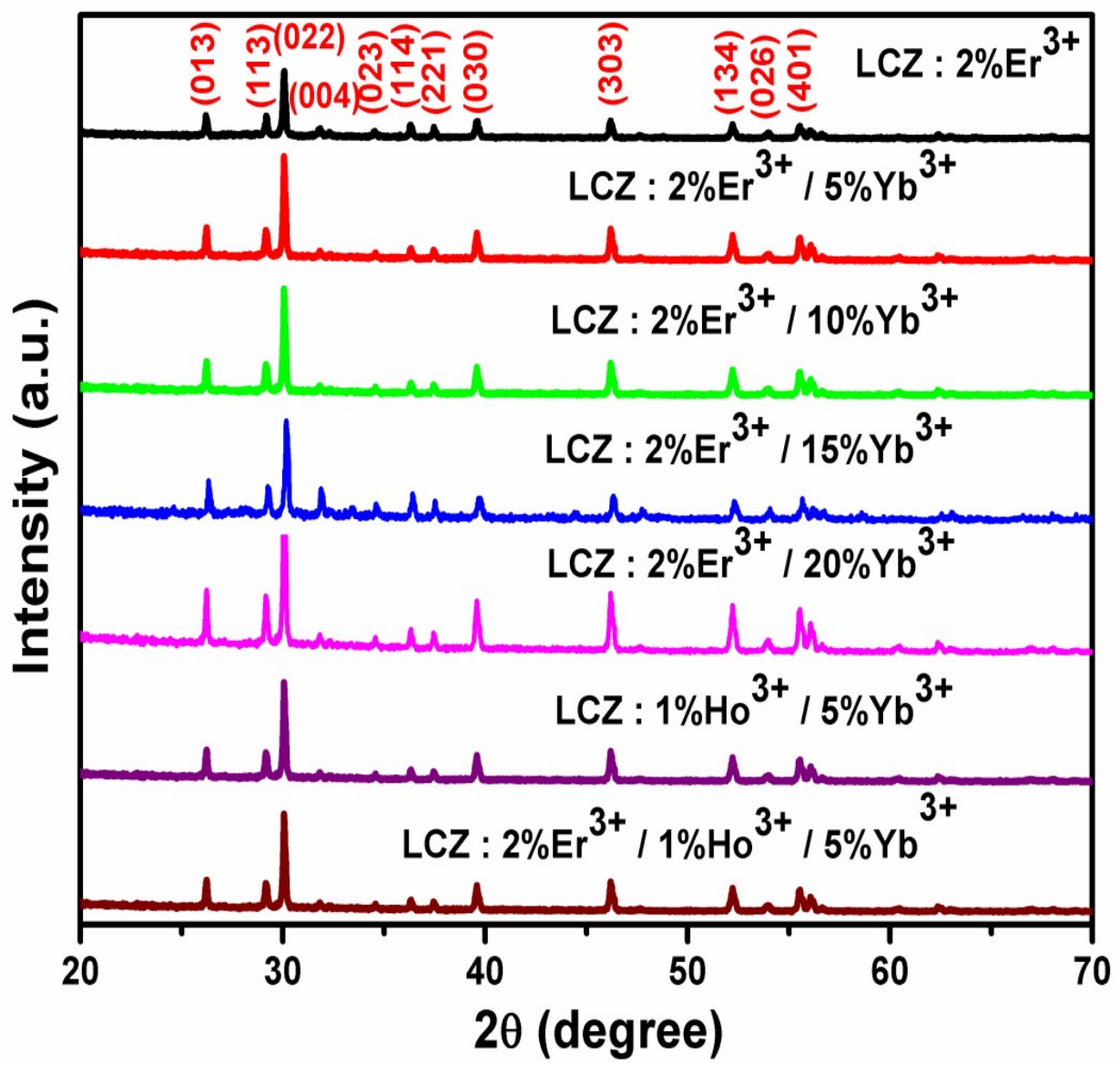

Fig. 1 XRD pattern of LCZ phosphor with varying RE concentration.

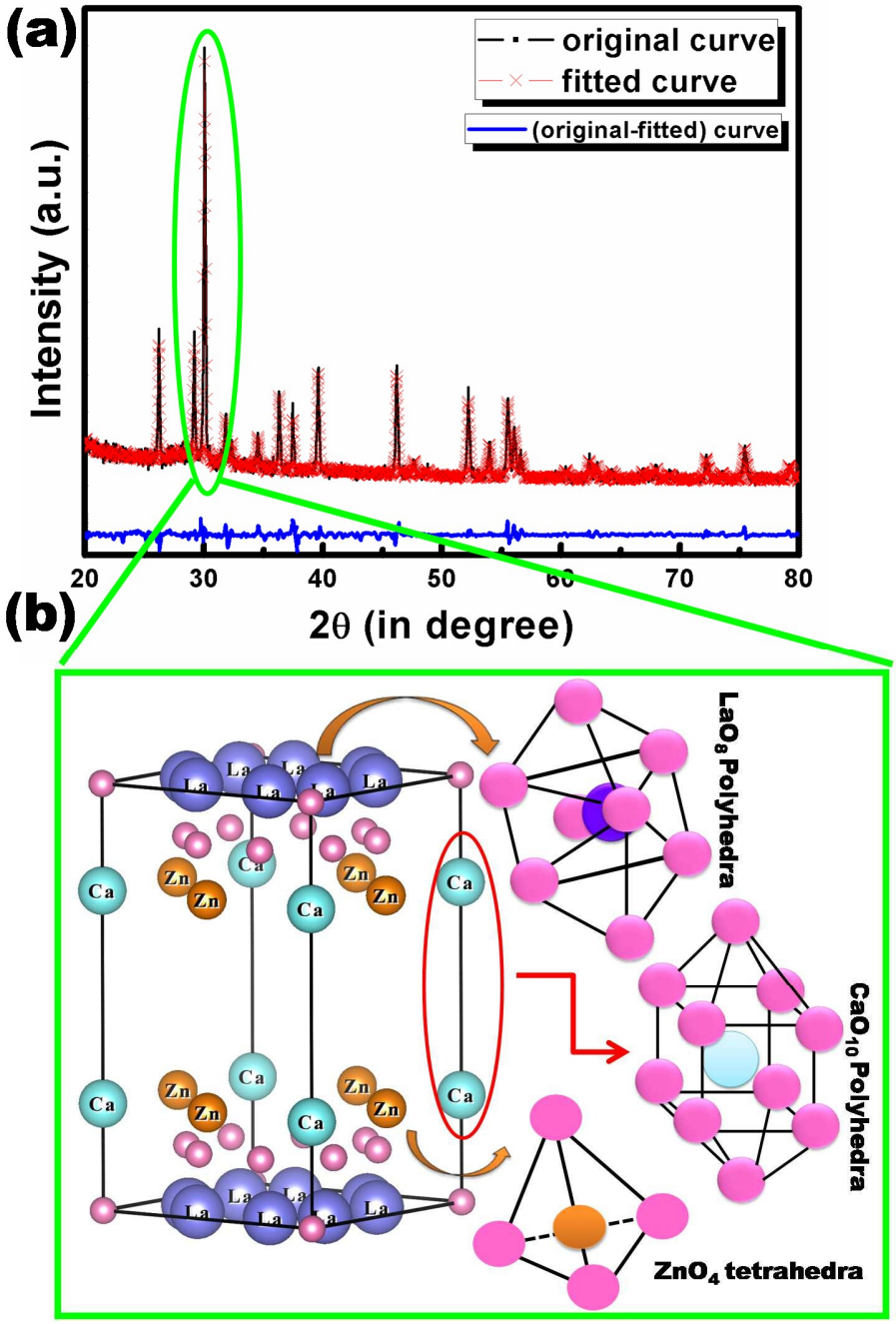

Fig. 2 (a) Fitted (×) and original (black line) powder XRD pattern of La_2CaZnO_5 phosphors and residuals (blue line in the bottom) for the structure refinement by the Rietveld method using the EXPO Program. (b) Schematic diagram of the La_2CaZnO_5 complex structure drawn by VESTA software.

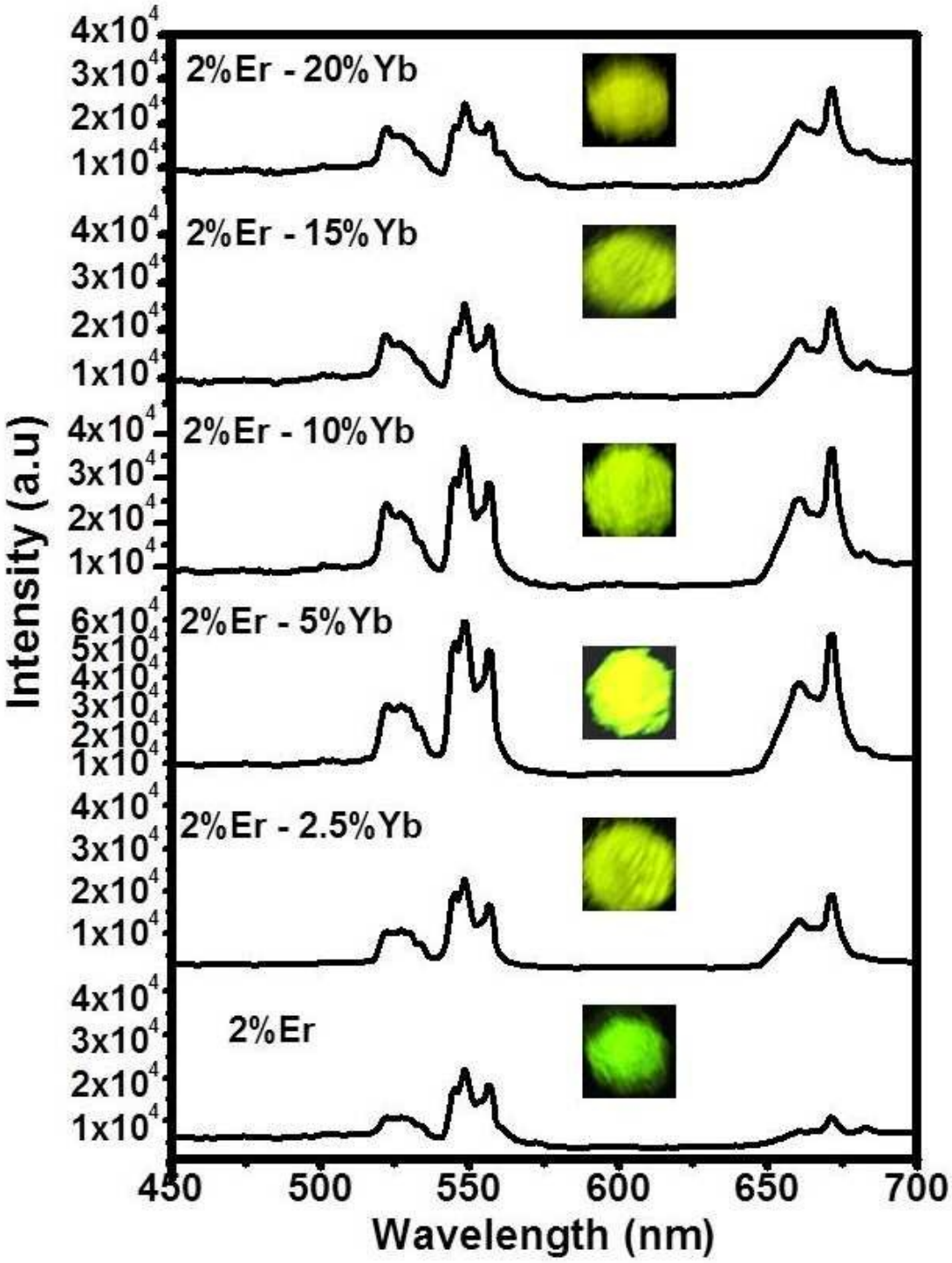

Fig. 3 UC spectra of LCZ phosphor with varying Er/ Yb concentration

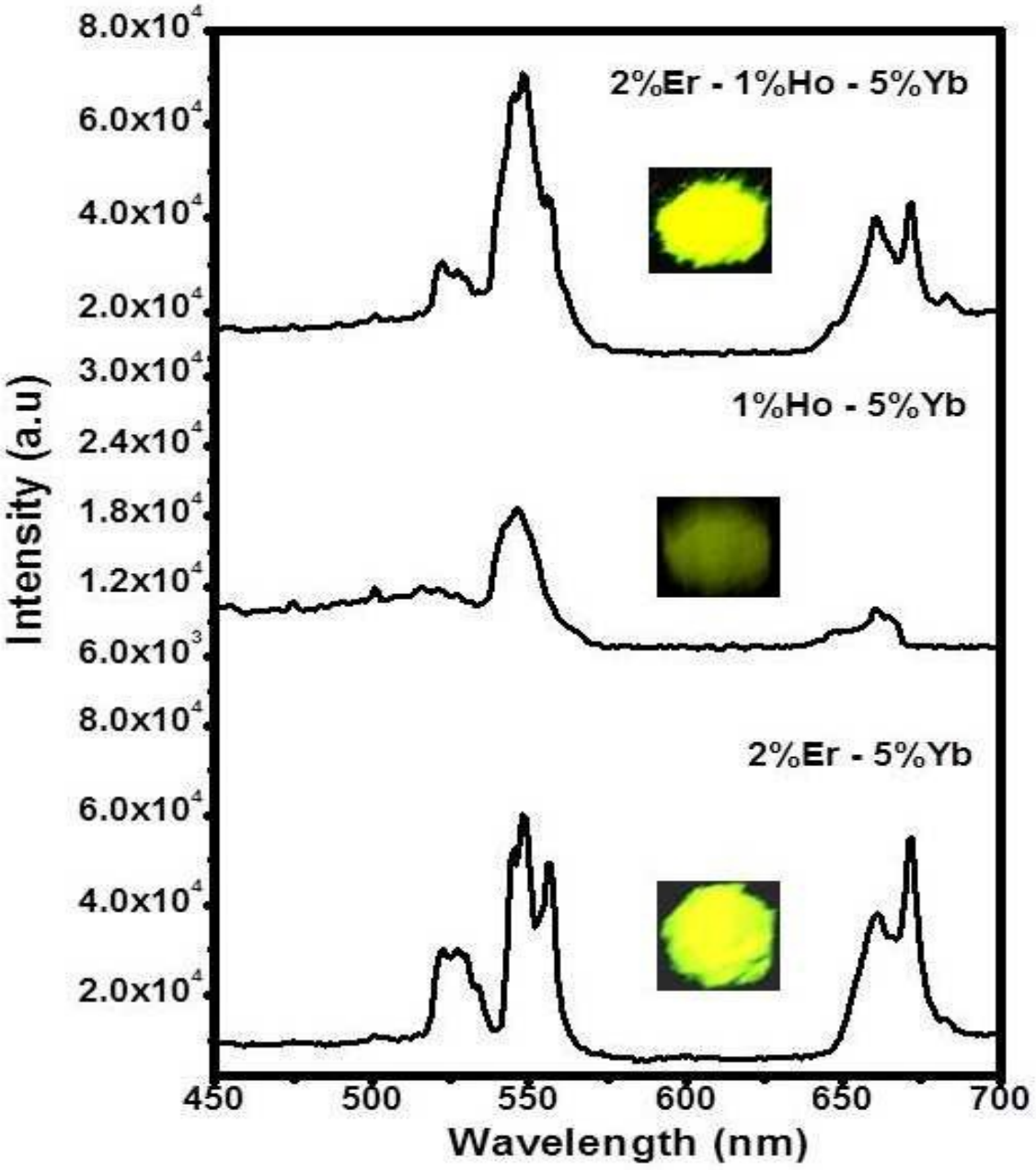

Fig. 4 Comparative UC spectra of LCZ phosphor with varying Er/ Ho/ Yb concentration

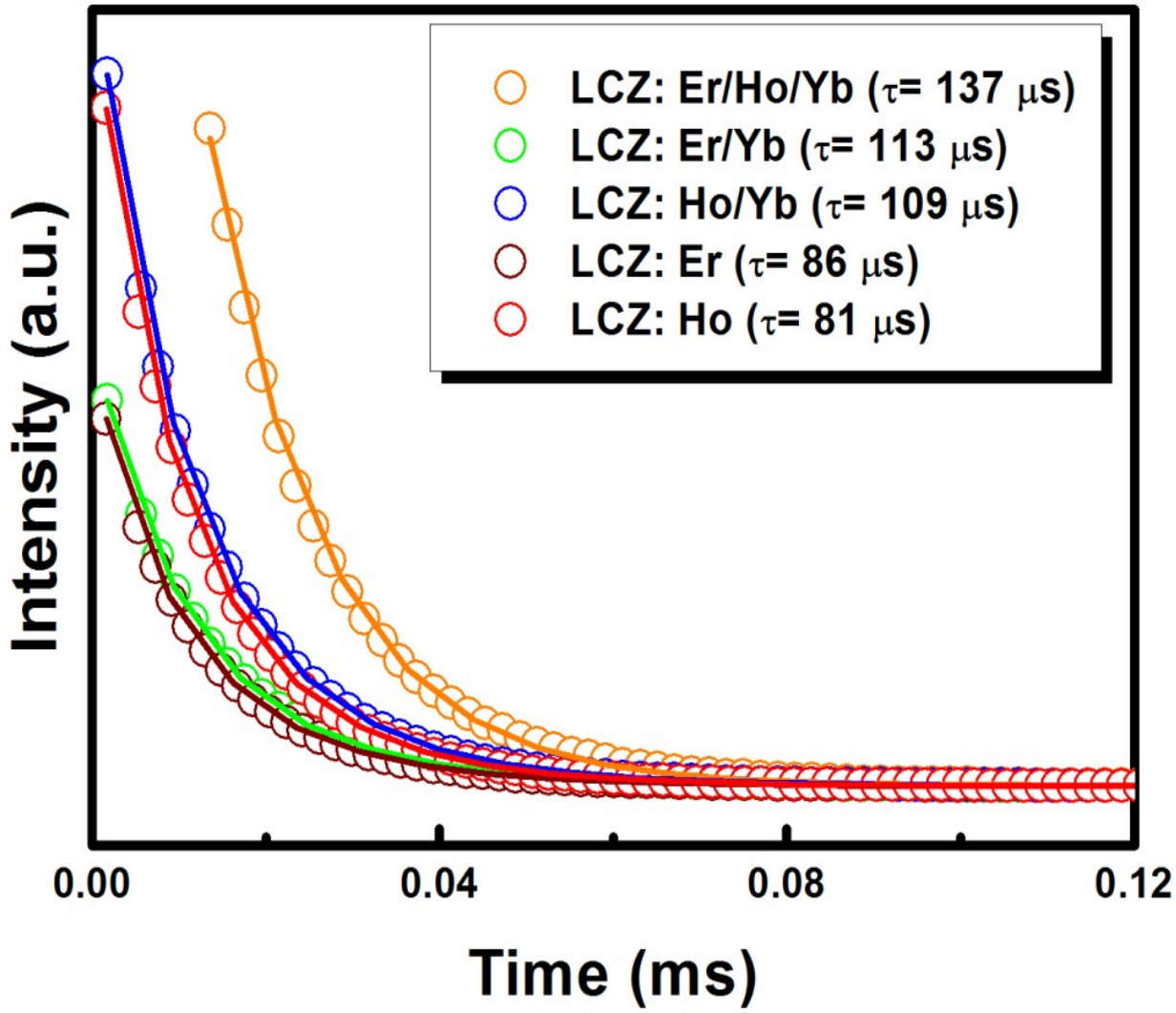

Fig. 5 Decay intensity as function of time of the green emission (548 nm) of the LCZ samples with different codoping ratios.

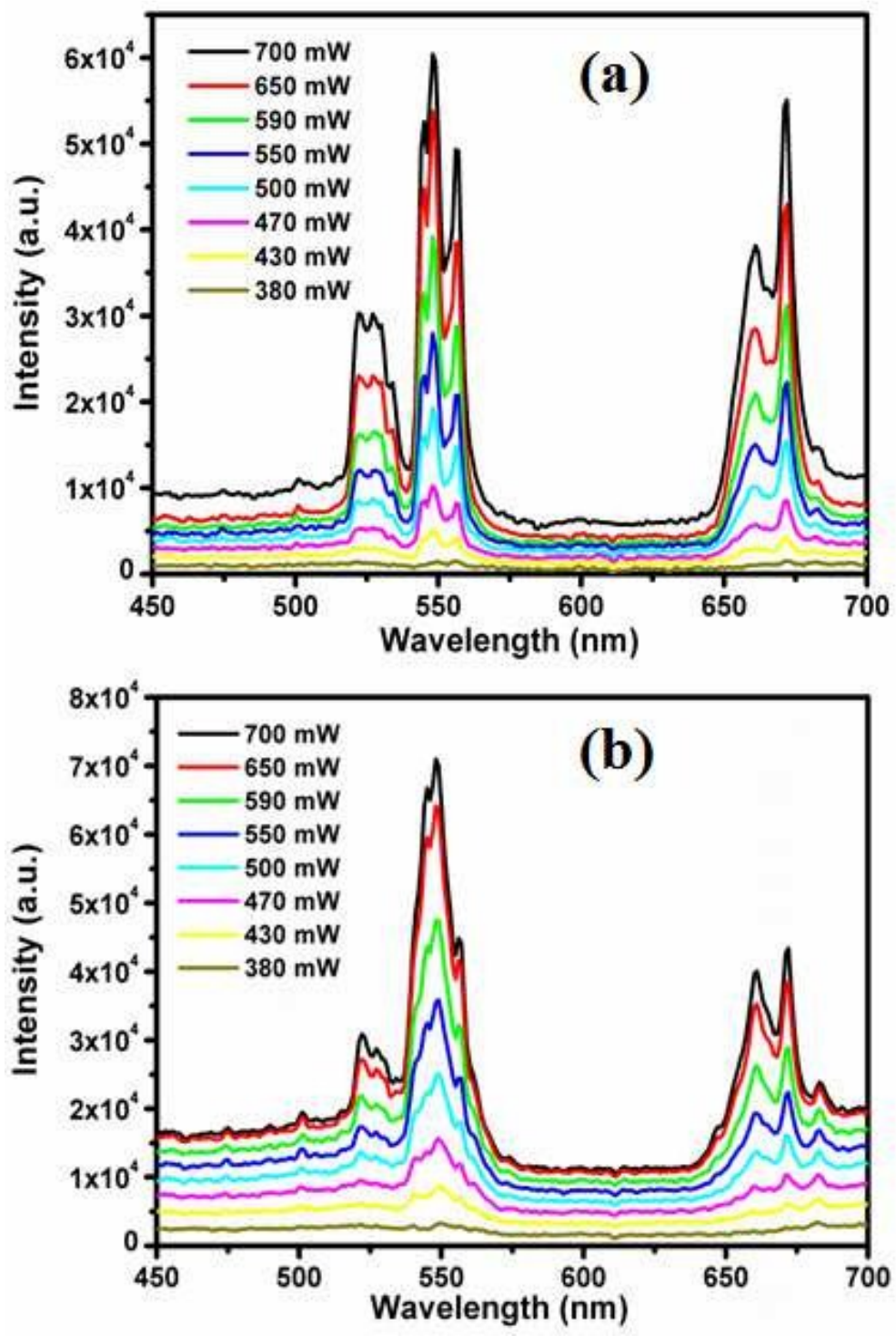

Fig. 6 Variation of UC intensity with the increment of the Laser Power for (a) LCZ: Er/ Yb and (b) LCZ: Er/ Ho/ Yb phosphors

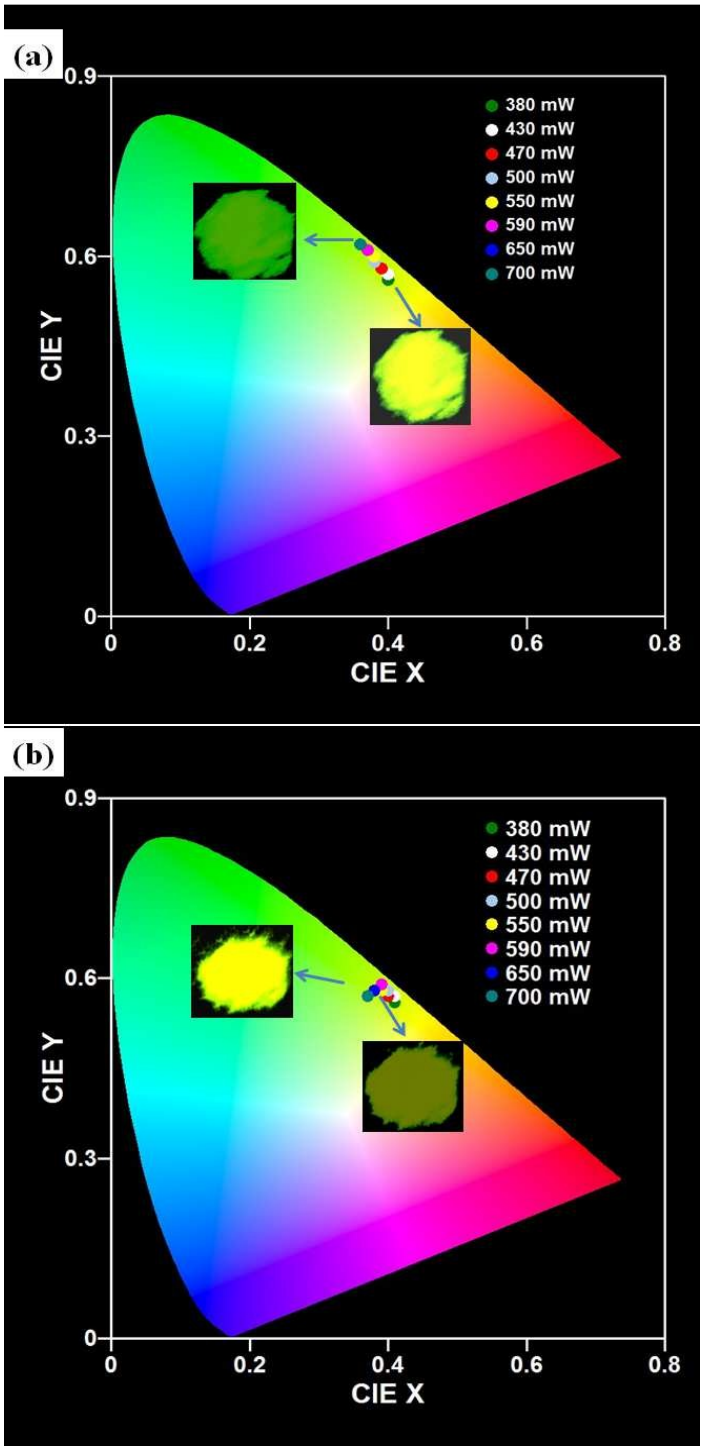

Fig. 7 Variation of colour coordinates with the increment of Laser Power for (a) LCZ: Er/ Yb and (b) LCZ: Er/ Ho/ Yb phosphors

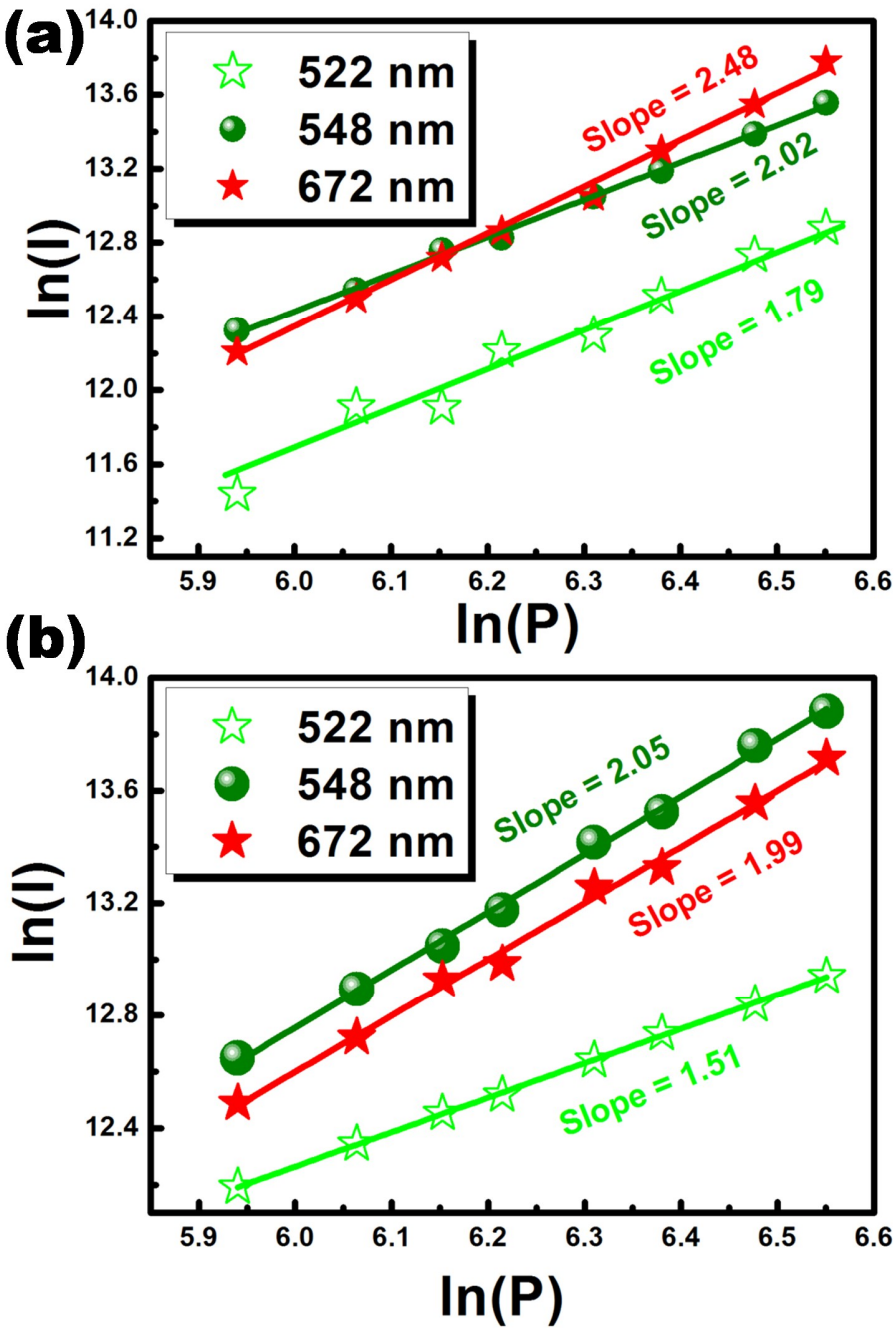

Fig. 8 Dependence of UC intensity with pumping Power for (a) LCZ: Er/ Yb and (b) LCZ: Er/ Ho/ Yb phosphors.

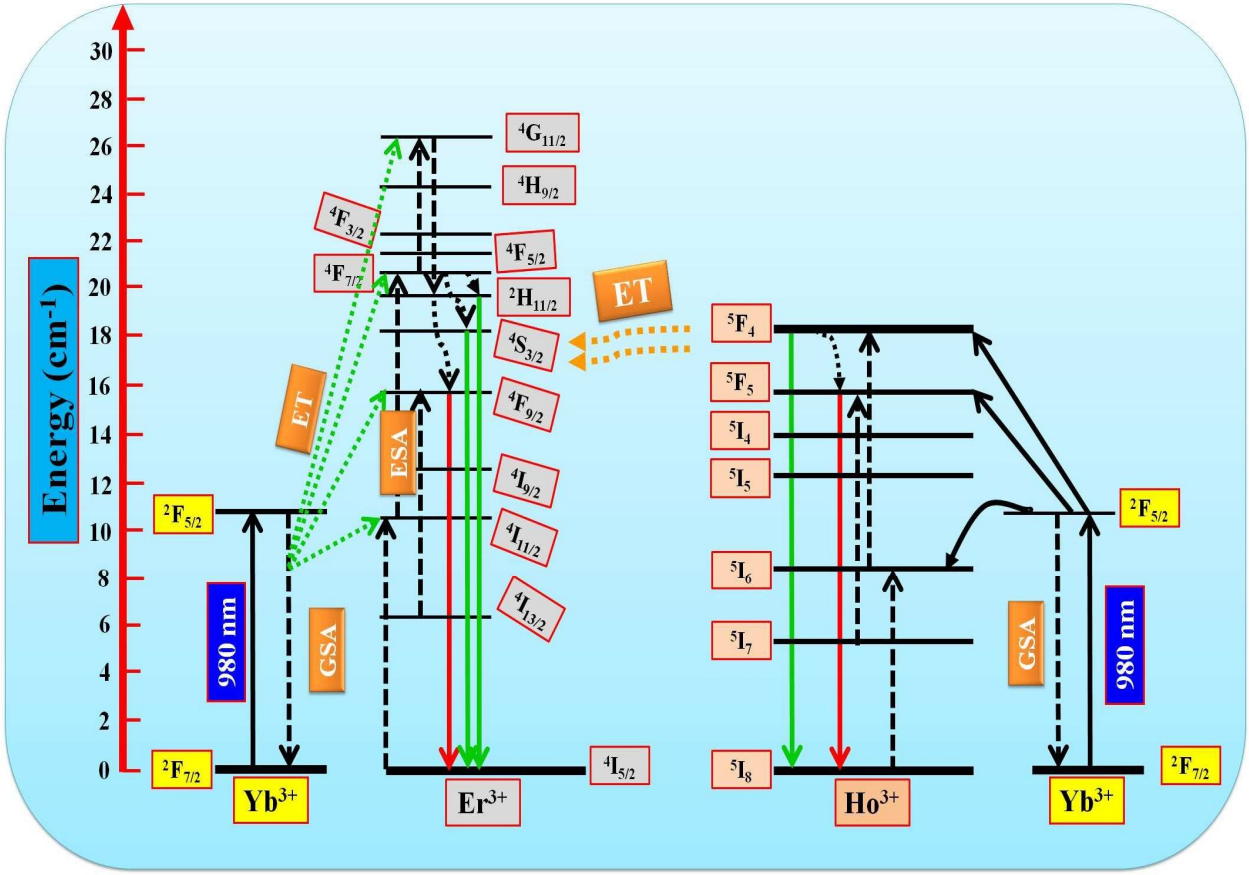

Fig. 9 Energy level diagram of Er^{3+}, Ho^{3+} and Yb^{3+} ions for various emissions of the La_2CaZnO_5 phosphor.

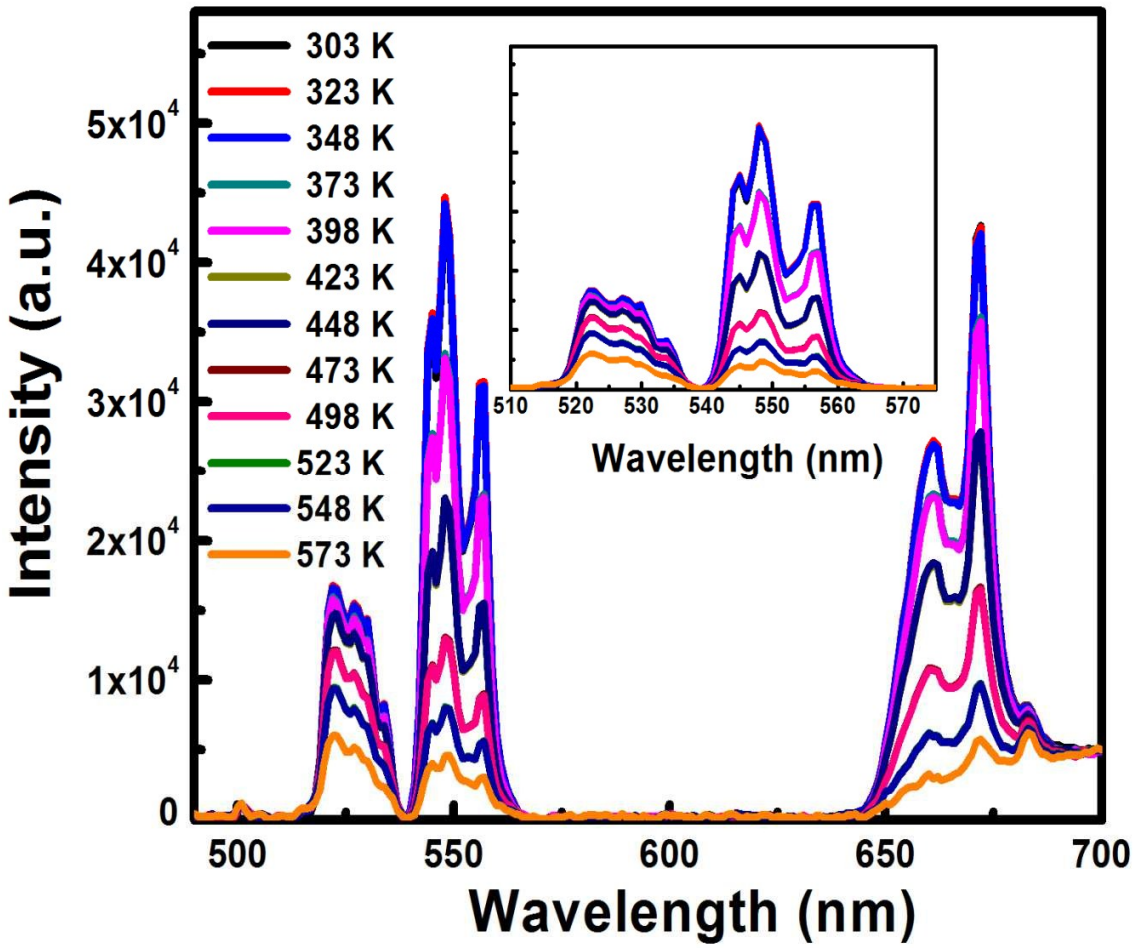

Fig. 10 Variation of UC spectra with temperature for La_2CaZnO_5: Er^{3+}/Yb^{3+} phosphor.

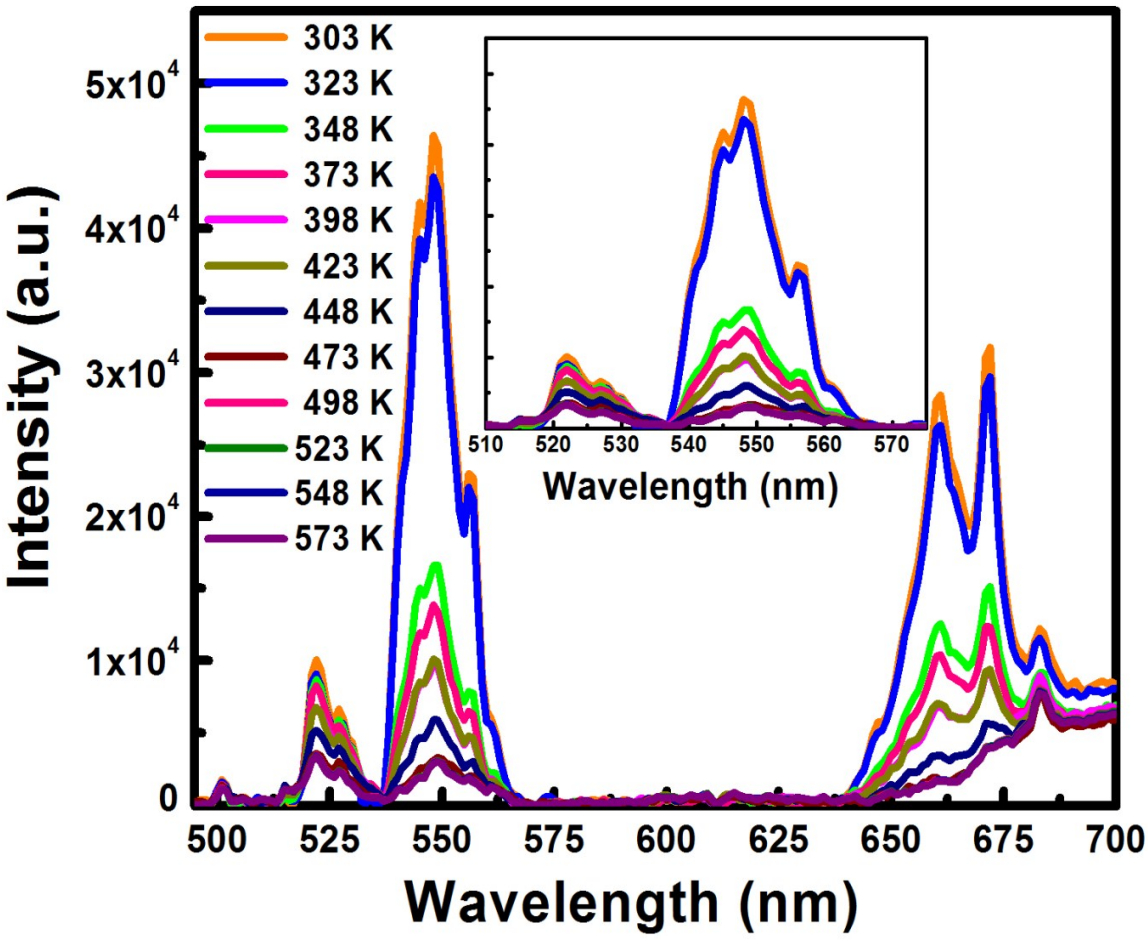

Fig. 11 Variation of UC spectra with temperature for La_2CaZnO_5: Er^{3+}/ Ho^{3+}/ Yb^{3+} phosphor.

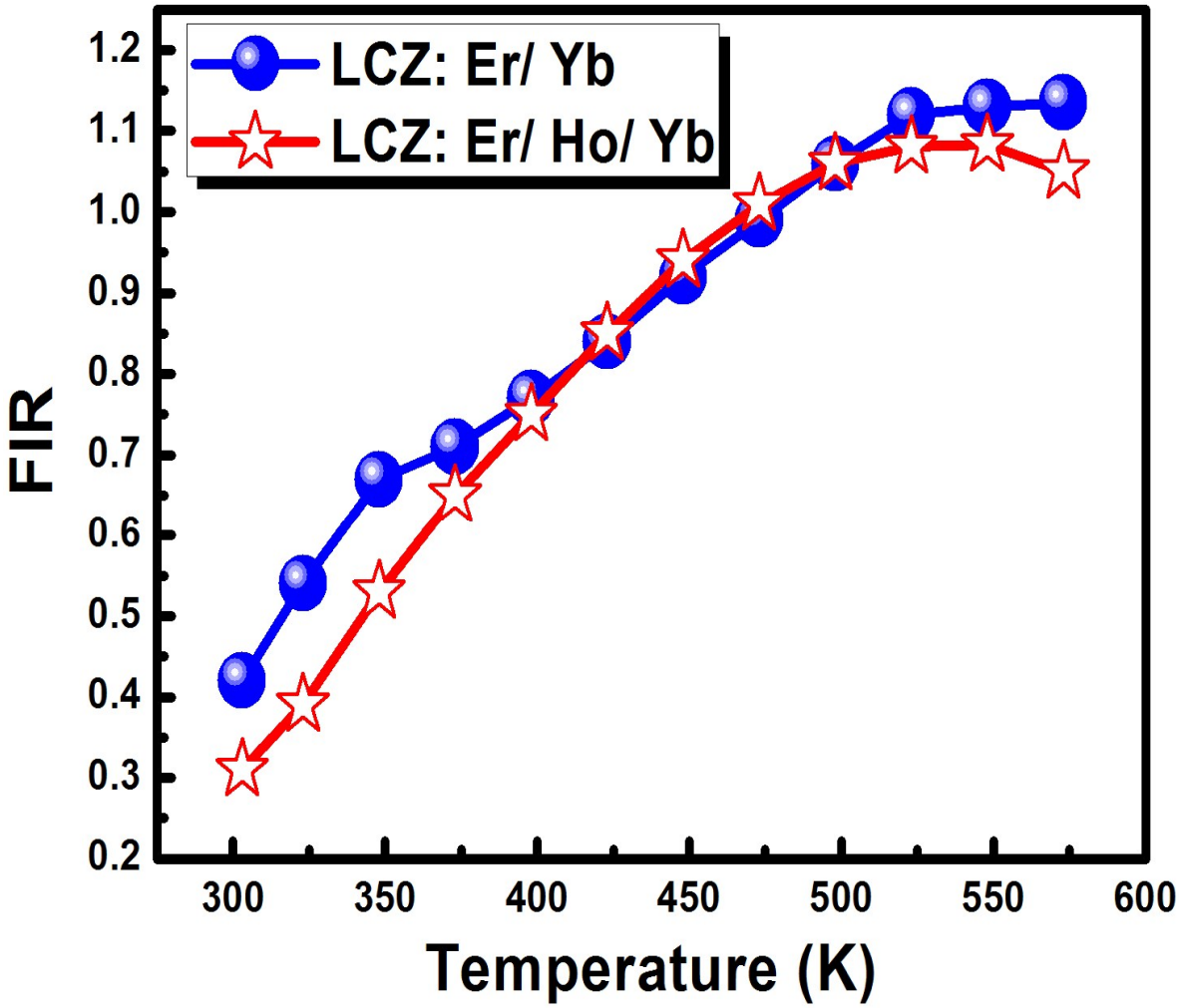

Fig. 12 Variation of FIR value of the green emission in LCZ host with different doping as a function with temperature.

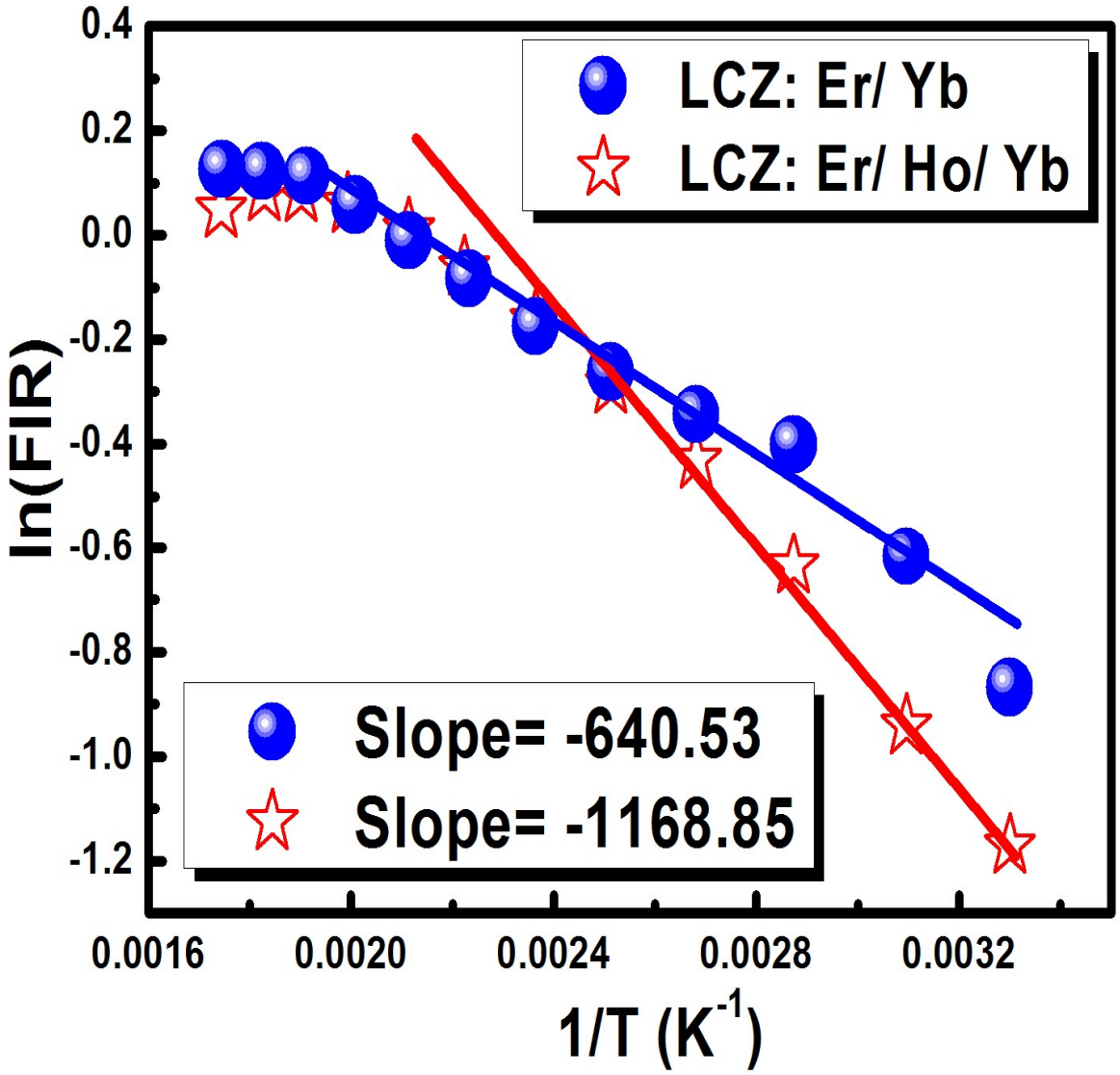

Fig. 13 Variation of logarithmic FIR value of the green emission in the LCZ host with inverse temperature.

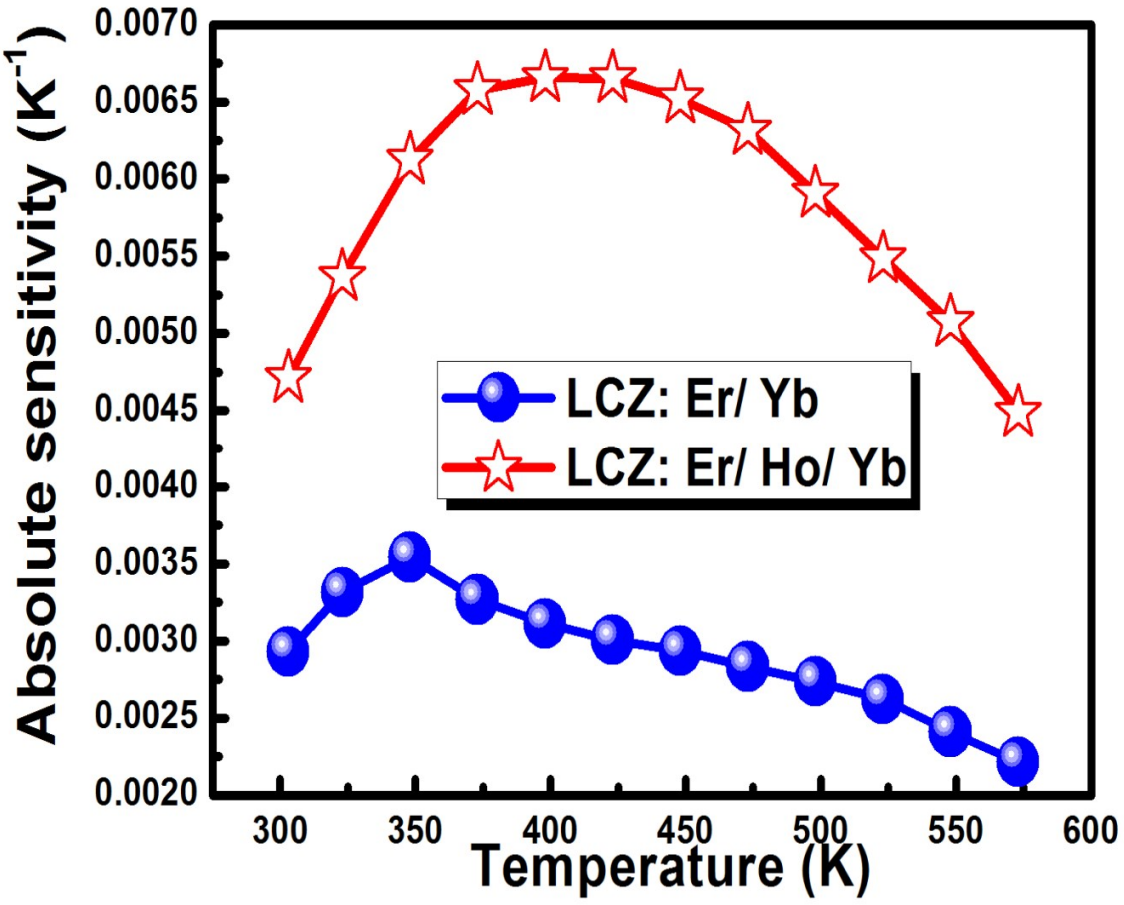

Fig. 14 Variation of absolute sensor sensitivity of the LCZ phosphors with temperature.

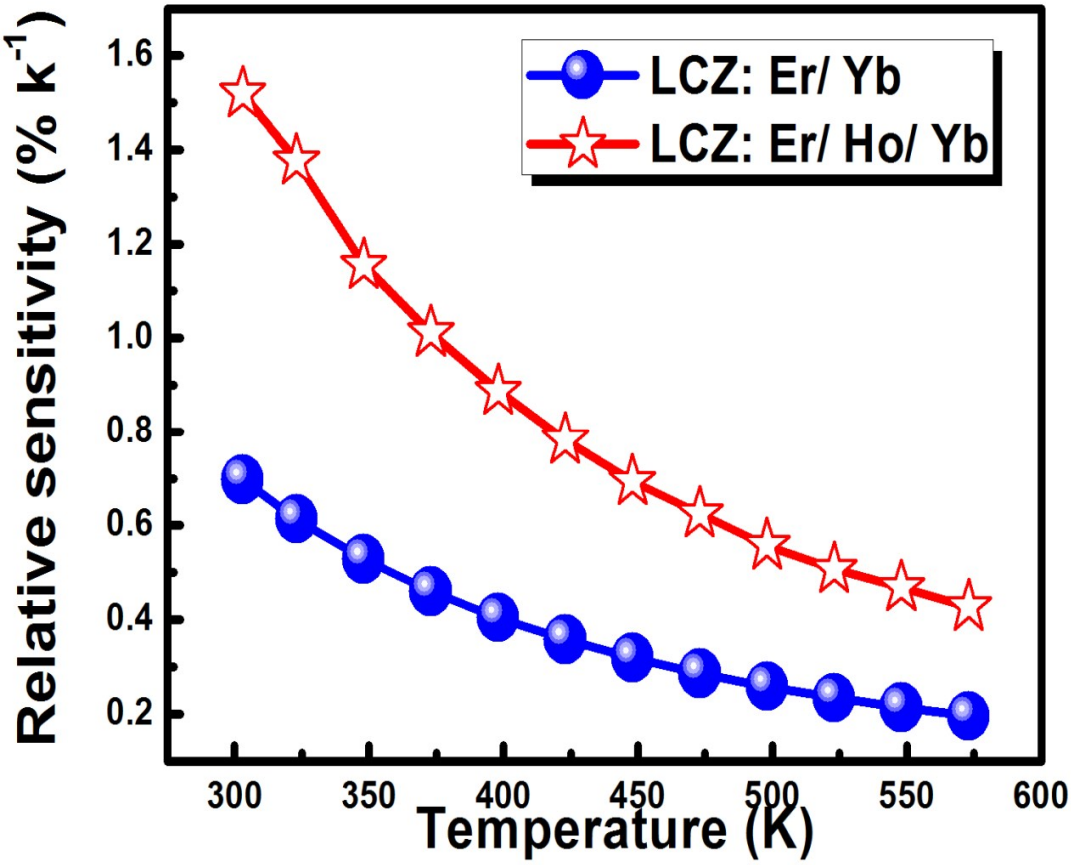

Fig. 15 Variation of relative sensor sensitivity of the LCZ phosphors with temperature.

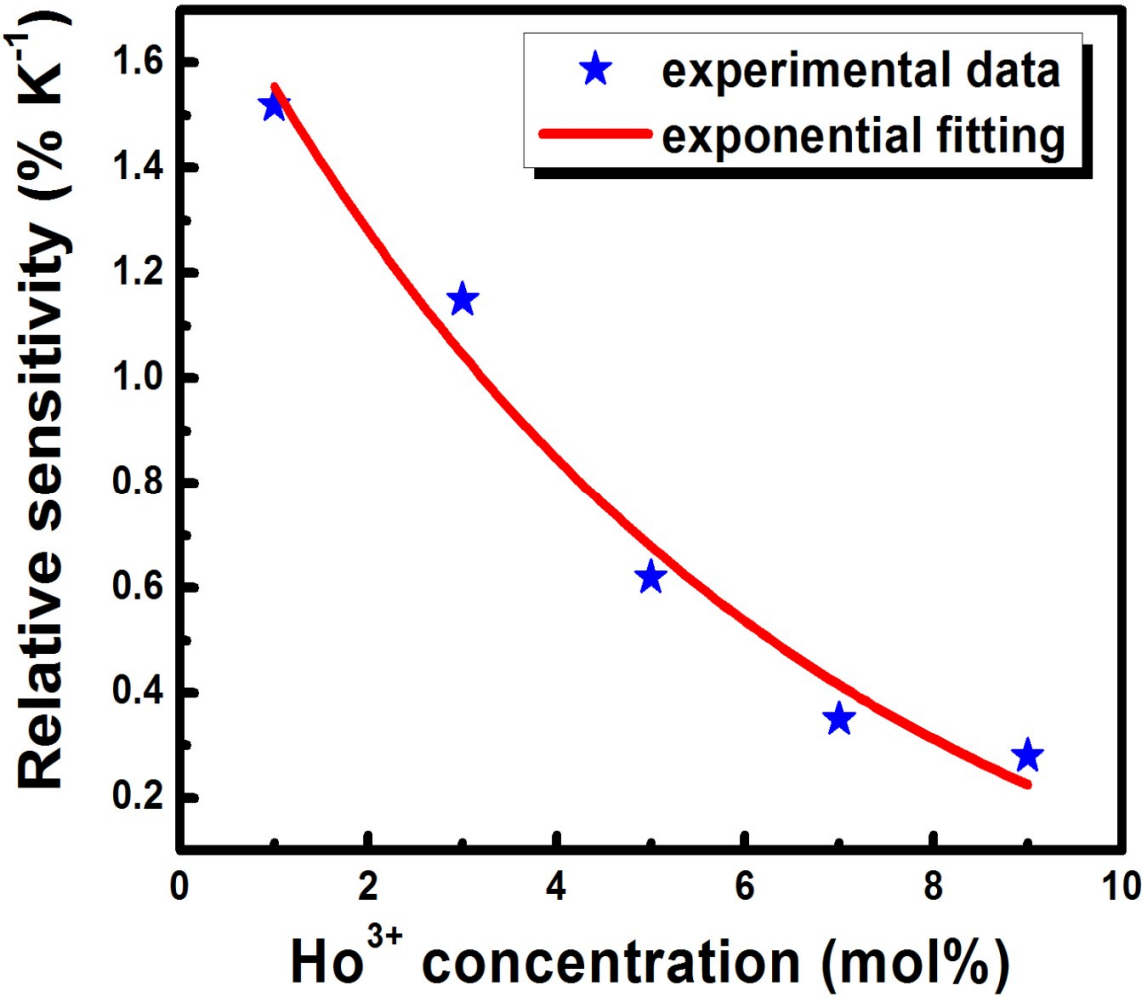

Fig. 16 Variation of relative sensor sensitivity of the LCZ phosphors with Ho^{3+} concentration.

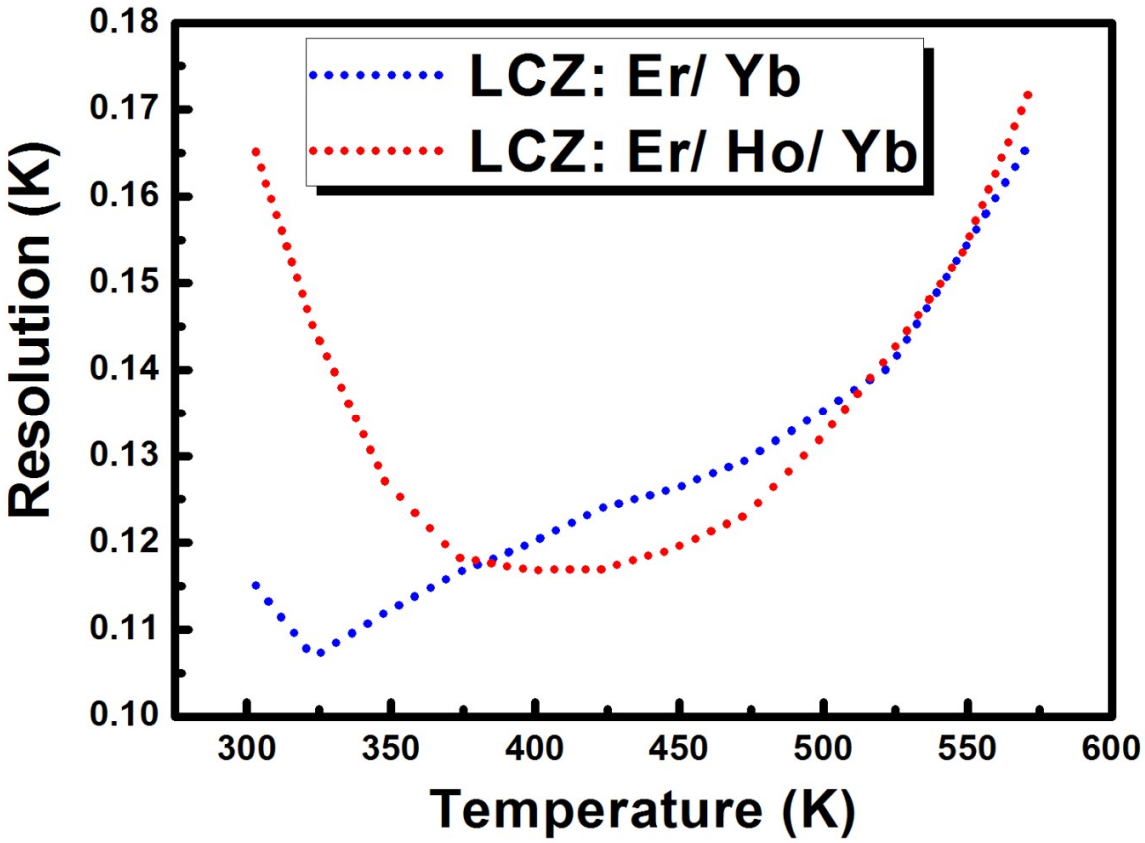

Fig. 17 Variation of resolution of the LCZ temperature sensor with temperature.

Tables:

Table 1: Refinement parameter obtained from FullProf Software.

Element	**x**	**y**	**z**	**Frac. occup.**
La (8p)	0.17363	0.67363	0.0	1.00
Zn (4i)	0.0	0.5	0.25	1.00
Ca (2g)	0.0	0.0	0.25	1.00
O(1) (1a)	0.0	0.0	0.0	1.00
O(2) (16u)	0.3519	0.8519	0.1376	1.00
a (Å)	7.0837			
c (Å)	11.8848			
R_{wp}, R_p, χ^2	7.36%, 5.89% and 3.92			
Space group	P 4/ m m m (tetragonal)			

Table 2 Comparative analysis of relative sensitivity and temperature range of the inorganic sensor materials.

S. No.	Phosphor	S_r at T_m	ΔT (T_m)	Ref.
1.	UC Nps: Er^{3+}/ Yb^{3+}	2.3	293- 318 (318)	31
2.	UC Nps: Tm^{3+}/ Yb^{3+}	0.2	293- 318 (315)	31
3.	$NaYF_4$: Er^{3+}/ Yb^{3+}	1.0	298- 318 (298)	20
4.	Gd_2O_3: Er^{3+}/ Yb^{3+}	0.2	295- 1000 (600)	32
5.	Fluoride glass: Er^{3+}/ Yb^{3+}	1.1	333- 375 (342)	33
6.	ZnO: Er^{3+}/ Yb^{3+}	0.6	273- 473 (273)	34
7.	LCZ: Er/ Yb	~ 0.51 (s= 0.0059 K^{-1})	298- 513 (483)	16
8.	LCZ: Er/ Yb	0.71 (s= 0.0036 K^{-1})	300- 573 (300)	Present work
9.	LCZ: Er/ Yb/ Ho	1.52 (s= 0.0067 K^{-1})	300- 573 (300)	Present work

Graphical and textual abstract

A series of Er^{3+}/Yb^{3+} and $Er^{3+}/Ho^{3+}/Yb^{3+}$ codoped $La_2Ca_2ZnO_5$ phosphors were prepared by the combustion synthesis method. The Er^{3+}/Yb^{3+}-codoped sample exhibited strong green and red upconversion (UC) emissions. The enhanced UC emission after codoping of Ho^{3+} was explained on the basis of energy exchange mechanisms between Er^{3+}/ Ho^{3+} and Yb^{3+} ions. Power dependence studies infer that the UC bands arose through a two/ three-photon absorption process. The high corresponding sensor responsiveness over a broad temperature range with large temperature resolution make the phosphors suitable for future applications in thermometry.